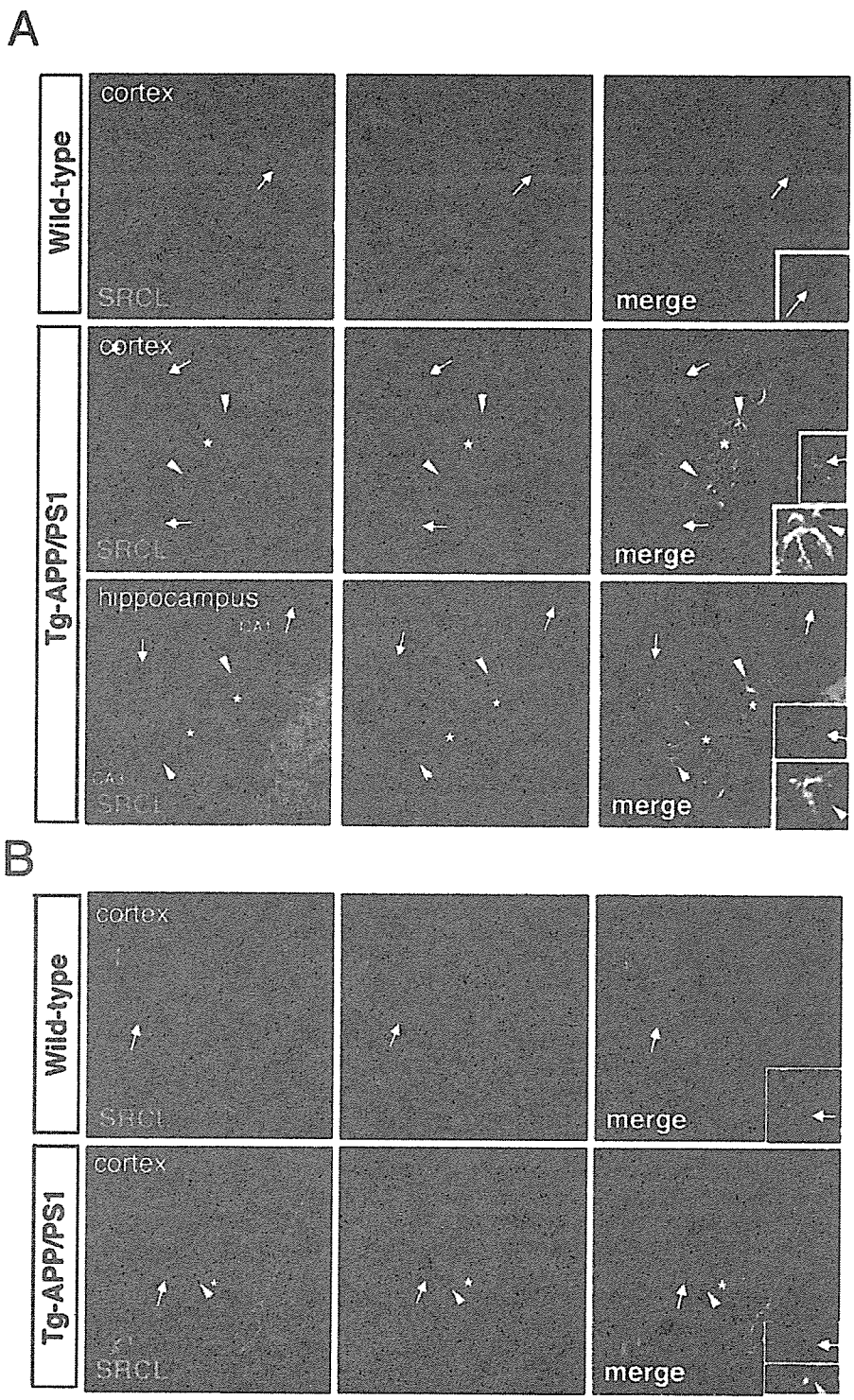

Fig. 5. Immunolocalization of SRCL in cerebral cortex and hippocampus of Tg-APP/PS1 mice and wild-type littermates. **A:** Paraffin sections from 9-month-old Tg-APP/PS1 mice and wild-type littermates were incubated with anti-SRCL and anti-GFAP primary antibodies, followed by their respective Alexa488 (green)- and Alexa546 (red)-conjugated secondary antibodies. Arrows point to cells immunopositive for GFAP only; and arrowheads, to those immunopositive for both SRCL and GFAP. CA1 and CA3 regions of the hippocampus are indicated. **B:** Frozen sections from cortex of a 9-month-old Tg-APP/PS1 and wild-type littermate were incubated with anti-SRCL and anti-Mac-1 primary antibodies, followed by their respective Alexa488 (green)- and Alexa546 (red)-conjugated secondary antibodies. Insets and asterisks in (A) and (B) show high-magnification views and Aβ plaques, respectively. GFAP, astrocytic marker; Mac-1, microglial marker. Arrows point to cells immunopositive for Mac-1 only; and arrowheads to cells immunopositive for both SRCL and Mac-1.

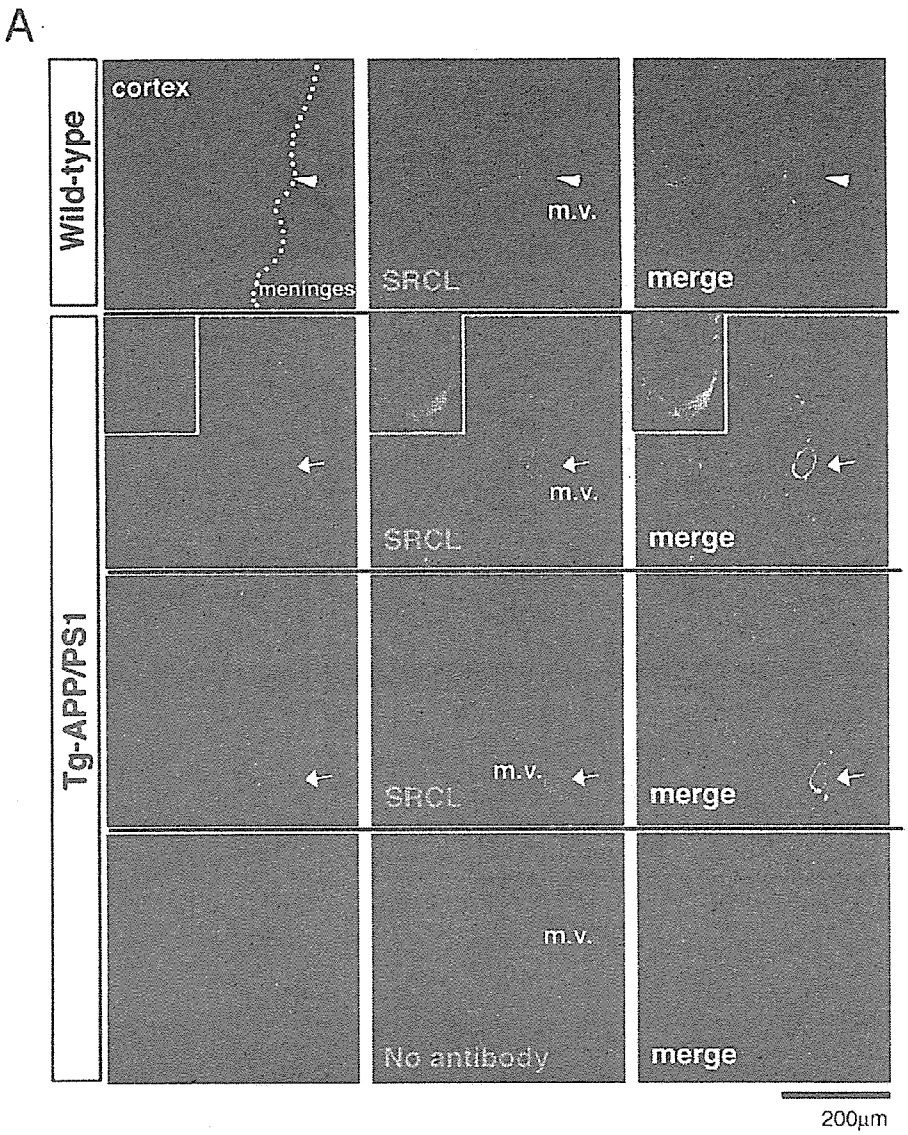

Fig. 6. Immunolocalization of SRCL in cortical vessels of Tg-APP/PS1 mice and wild-type littermates. **A:** Double-immunostaining for SRCL and Aβ in leptomeningeal vessels. Paraffin sections from the cortices of 9-month-old Tg-APP/PS1 mice and wild-type littermates were incubated with rabbit anti-$A\beta_{1-40/1-42}$ and rabbit anti-SRCL antibodies, pre-labeled with Alexa546 (red) and Alexa488 (green), respectively, by using a Zenon rabbit IgG Labeling Kit (Invitrogen), respectively, and counterstained with Hoechst33342 (blue) to visualize nuclei. Arrowheads indicate a meningeal vessel without Aβ-IR or SRCL-IR. Arrows indicate Aβ/SRCL-double positive vessels. Inset, a high-magnification view. Lowest panel represents control immunostaining without anti-SRCL antibody. m.v., meningeal vessel (leptomeningeal vessel). **B:** Schematic representation showing vascular/perivascular cells of leptomeningeal vessels (m.v.). In wild-type mice, thin ECs and SMCs are seen. Beside the vessel, a perivascular macrophage (MATO cell) is seen. In Tg-APP/PS1, thickness of the vessel has increased, and the number of SMCs has increased and many macrophages has infiltrated into the vascular wall. Red color shows the Aβ aggregates in the extracellular matrix and the Aβ particles ingested by the cells. MATO, MATO cell (perivascular macrophage, yellow); SMC, smooth muscle cell (orange); EC, endothelial cell (light green); MØ, macrophages (yellow). **C:** Representative pictures of double-immunostaining for SRCL and CD31, αSMA or GFAP in leptomeningeal vessels. Paraffin sections from cortices of 9-month-old Tg-APP/PS1 mice and wild-type littermates were immunostained with anti-SRCL and anti-rat CD31 (for activated microglia/macrophage including MATO cells and ECs; Lewis rat activated microglia as immunogen), anti-GFAP (for astrocytes) or anti-αSMA (for SMCs) as primary antibody, followed by their respective Alexa488 (green)- and Alexa546 (red)-conjugated secondary antibodies. Sections were counterstained with Hoechst33342 (blue). m.v., leptomeningeal vessel. Arrows indicate CD31-positive ECs. **D:** Magnified views of double-immunostaining for SRCL and CD31 or αSMA of leptomeningeal vessels in 9-month-old Tg-APP/PS. Paraffin sections were processed for immunostaining with anti-SRCL, CD31 or αSMA as described above. **E:** Representative photo of double-immunostaining for SRCL and GFAP in cortical tissues associated with amyloid plaques (asterisks) and cortical amyloid angiopathy in a 9-month-old Tg-APP/PS1. Paraffin sections were processed for immunostaining using anti-GFAP and anti-SRCL primary antibodies, followed by their respective Alexa546 (red)- and Alexa488 (green)-conjugated secondary antibodies. Intra-cortical vessel is indicated as "c.v." at the right bottom corner of the merged view. Asterisks indicate amyloid plaques.

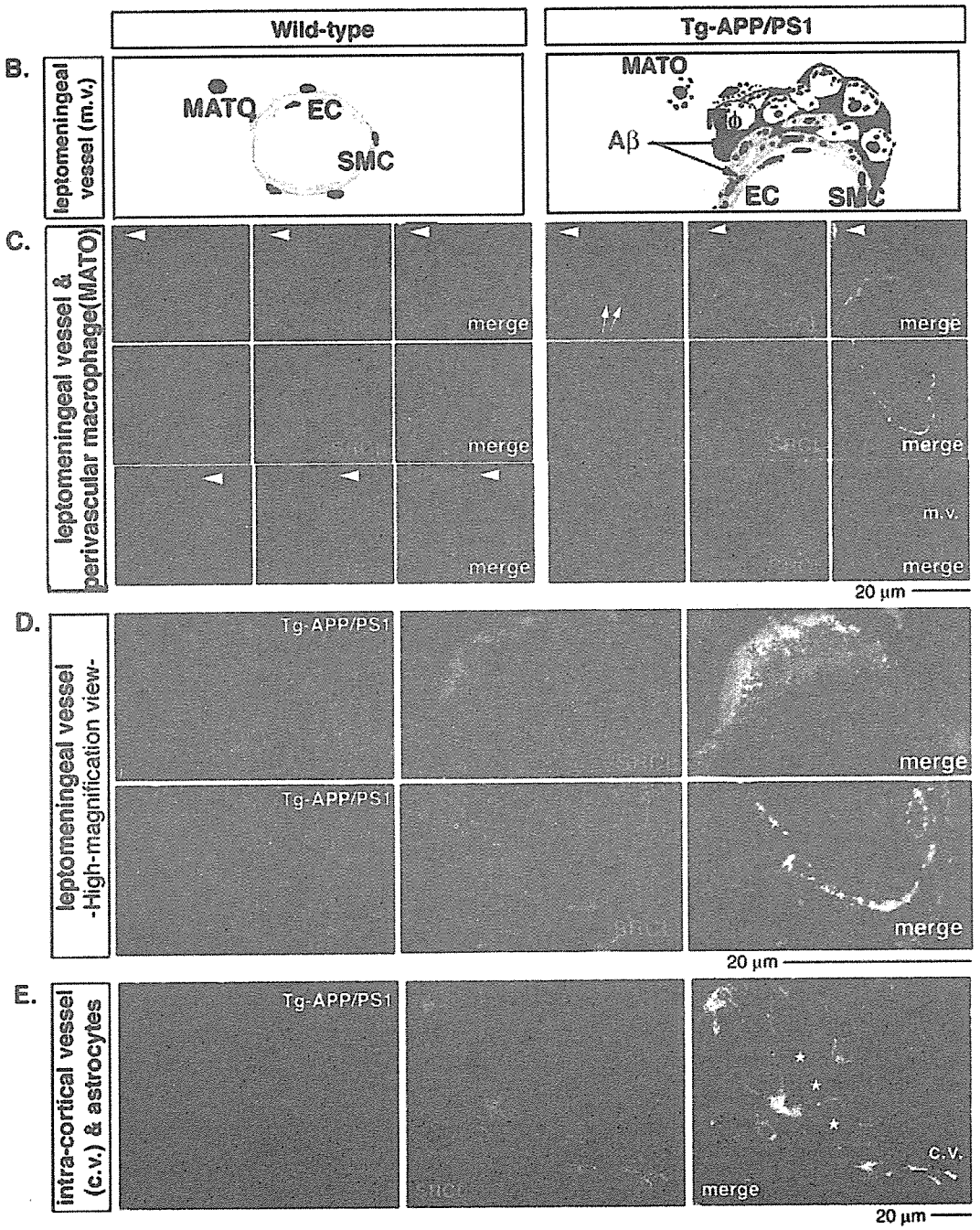

Figure 6. (Continued).

positive SMCs (red) in Tg-APP/PS1 mice (Fig. 6C, middle panel). At high-magnification (Fig. 6D, lower panel), SRCL-IR appeared as multiple particles colocalized with αSMA-IR inside cells, indicating that SMCs of Tg-APP/PS1 also internalized SRCL. We observed strong induction of SRCL-IR (green) within both GFAP-positive astrocytic cell bodies (red) and their end feet (red) surrounding a cortical vessel (c.v.) associated with cerebral amyloid angiopathy (CAA) in Tg-APP/PS1 (Fig. 6E). The astrocytes associated with Aβ-plaques (asterisks) expressed SRCL-IR predominantly intracellularly, suggesting the internalization, of Aβ by SRCL in

astrocytes. Interestingly, we could occasionally observe astrocytes that extended their feet toward both an amyloid plaque (asterisk) and cortical micro-vessels (c.v.). This finding may suggest a possible role of astrocytic SRCL for Aβ clearance by transfer from amyloid plaque to the systemic circulation via c.v.

In brief summary, immunostaining results showed that, in wild-type littermates, SRCL-IR was present in MATO cells and to a lesser extent in SMCs, whereas SRCL-IR was markedly induced and colocalized with $fA\beta_{1-40/1-42}$-IR as particles inside the vascular wall. Within the vascular/perivascular cells, SRCL was induced in infiltrating macrophages, MATO cells, SMCs, ECs and astrocytes in Tg-APP/PS1, thus raising the possibility that upregulated SRCL in subpopulations of vascular/perivascular cells may play an important role in the binding, and presumably the clearance, of Aβ in the Tg-APP/PS1 brain.

Real-Time RT-PCR Shows the Expression of SRCL in the Brain of Patients With AD

To assess the expression and localization of SRCL in the brains of AD patients, we examined *SRCL* mRNA expression in autopsy samples from patients with AD and control subjects listed in Figure 7A. Although the number of autopsy samples was limited and thus insufficient for statistical analysis, quantitative real-time RT-PCR showed a tendency for an increase in the level of the *SRCL* mRNA in the cortical tissues of AD patients compared to the level in the control subjects (Fig. 7B), suggesting a role for SRCL in AD brain.

Expression of hSRCL in Brains of Patients With AD

We investigated the immunolocalization of SRCL in the temporal cortex of patients with AD. A large number of SRCL-IR cells were present in AD brain tissues, whereas SRCL-IR cells were rare in control samples (Fig. 8A). Using SRCL/GFAP-double immunostaining, we observed that strong SRCL-IR (pink) was colocalized with GFAP-IR (brown) in plaque (black asterisks)-surrounding reactive astrocytes and in perivascular astrocytic end-feet (brown) associated with CAA (green asterisks) in the temporal cortex of AD-affected brains (Fig. 8B). At high magnification, SRCL-IR appeared as particles within the cells (Fig. 8B, right panel). Furthermore, when we stained for SRCL and Iba-1 (for microglia/macrophages including MATO cells), SRCL-IR (pink) was found in some Iba1-positive activated microglia (arrows) or vascular macrophages and MATO cells (arrowhead) in the AD-affected brains (Fig. 8C). In addition, double immunostaining for SRCL (pink) and $A\beta_{1-40/1-42}$ (brown) showed that SRCL-IR was colocalized with Aβ as multiple particles in intracellular compartments of vascular cells, such as infiltrating macrophages, SMCs, and some ECs in the AD samples (Fig. 8D,E, in green arrowheads) consistent with the findings in Tg-APP/PS1 (Fig. 6A,D). The specificity of SRCL-IR was confirmed by pre-absorbing the antibody with its immunogen (Fig. 8F).

A

Disorder	Age	Sex	Cause of death
Control	79	F	drug overdose
Control	71	F	multiple medical disorder
Control	20	M	multiple injuries
AD	81	M	complication of AD
AD	87	F	heart disease
AD	86	F	complication of AD
AD	83	F	complication of AD

B

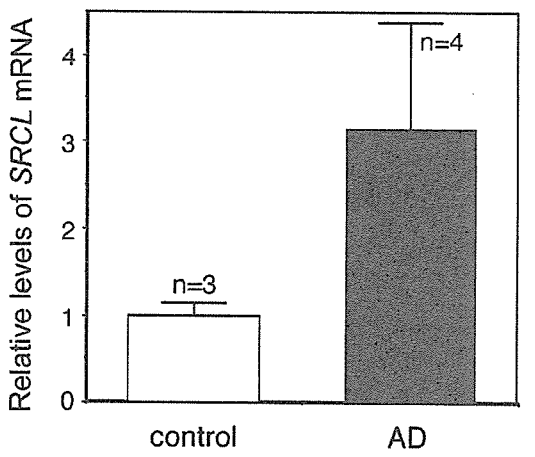

Fig. 7. Expression of *hSRCL* mRNA in brains of AD patients. **A:** Summary of autopsy samples used for analysis of *hSRCL* mRNA expression. **B:** Quantitative real-time RT-PCR of *hSRCL* mRNA from the temporal cortex of control subjects and AD patients. The *hSRCL* mRNA level was expressed as the ratio to that of *GAPDH* mRNA. Scale bar = ±SE (standard error).

In brief summary, in AD-brains, SRCL-IR appeared as numerous particles inside plaque-associated reactive astrocytes, activated microglia, and vascular/perivascular cells, such as the infiltrating macrophages within the vessel wall, SMCs and ECs that were associated with CAA and was consistent with our findings in Tg-APP/PS1 mice. Our findings thus suggest that upregulated SRCL on reactive astrocytes, activated microglia, and vascular/perivascular cells might be involved in Aβ binding and clearance in AD.

DISCUSSION

The accumulation of fibrillar Aβ (fAβ) is an important component of AD pathogenesis, a disease that

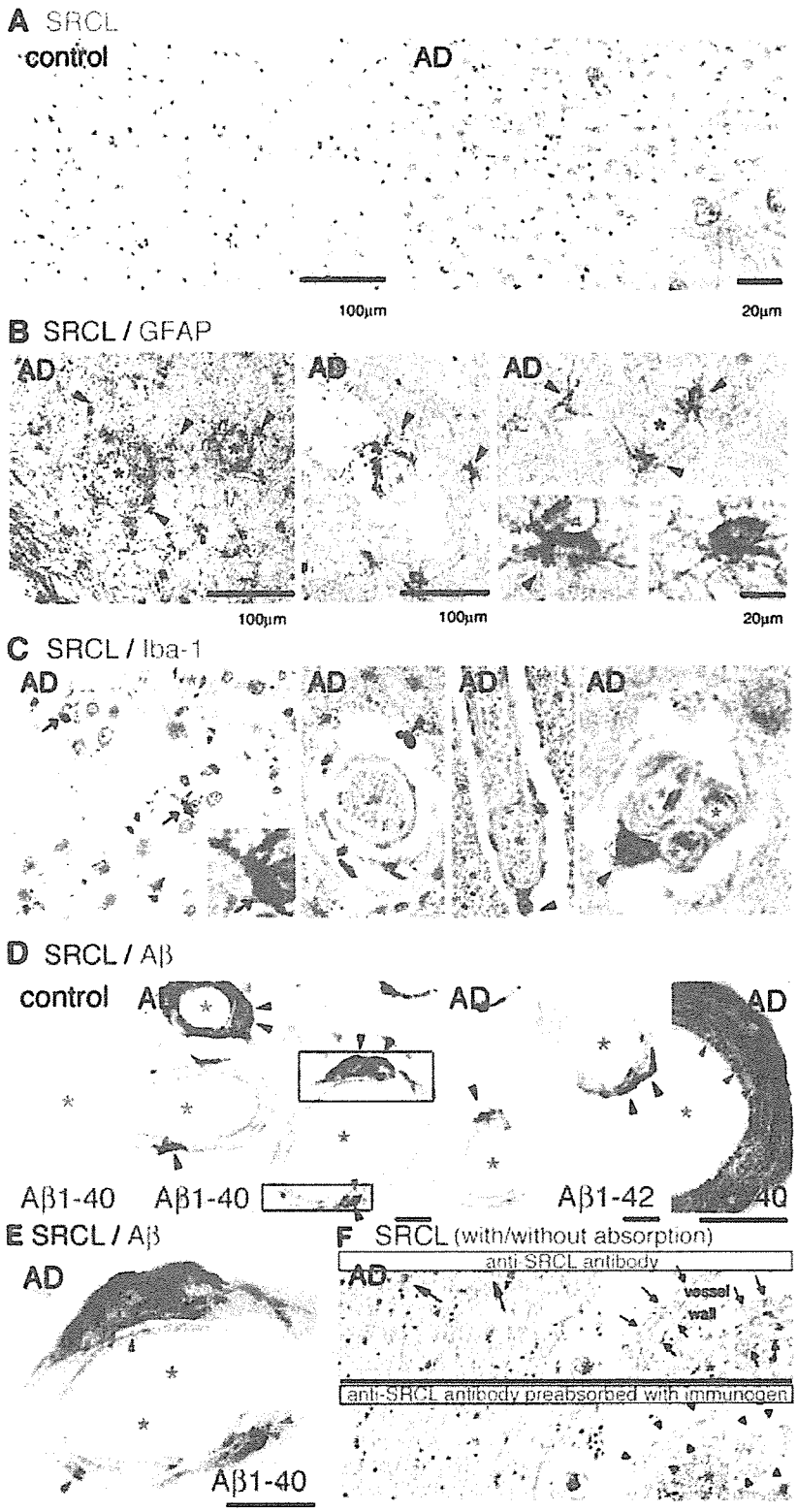

Fig. 8. Immunostaining for hSRCL in the temporal cortex of AD patients. Formalin-fixed human brain tissues from control subjects and AD patients were embedded in paraffin, deparaffinized, sectioned thinly, and used for immunostaining. **A:** Brain tissues of controls and AD patients immunostained with anti-SRCL antibody recognizing hSRCL. Immunoreactivity was visualized by using DAB (brown color). **B:** Double-immunostaining for hSRCL (pink) and GFAP (brown). Arrowheads indicate hSRCL-IR astrocytes surrounding Aβ deposits (black asterisks). Green asterisk, intra-cortical vessel. **C:** Double-immunostaining of hSRCL (pink) and Iba-1 (brown), a marker for microglia/macrophages. Arrows indicate hSRCL-IR microglial cells. Arrowheads indicate hSRCL-IR-MATO cells. **D:** Double-immunostaining of hSRCL (pink) and $A\beta_{1-42}$ (brown) in a vessel associated with CAA. Green asterisks and green arrowheads indicate vessels and hSRCL/Aβ double-positive particles, respectively. Scale bars = 20 μm. **E:** High-magnification views of rectangular areas shown in second panel of (D). Scale bar = 20 μm. Green arrowheads indicate SRCL/Aβ double positive particles; and green asterisks indicate intravascular spaces of leptomeningeal vessel. **F:** Absorption test. Immunostaining for hSRCL (brown) with or without preabsorption with immunogen. Black arrows show cells with hSRCL-IR. Black arrowheads indicate cells, the hSRCL-IR of which was eliminated by preabsorption with immunogen.

causes significant morbidity and mortality in adult populations. We wished to determine factors that may modulate accumulation of Aβ in vivo, and focused our attention on the clearance of Aβ by SRCL. Clearly, SRCL was expressed in the brains of AD patients, and SRCL could bind fAβ. RT-PCR showed that SRCL was expressed in neonatal astrocytes and microglia in tissue culture, and that *SRCL* mRNA levels increased after increased microglial activation. In addition, SRCL levels increased in neonatal astrocytes treated with fAβ in vitro. These in vitro data are consistent with immunohistochemical findings. In control mice and human subjects, SRCL-IR was below the detection limits in astrocytes, microglia and macrophages except perivascular macrophages (MATO cells). SRCL-IR intensity was elevated in most of the Aβ-positive astrocytes and in some of the Aβ-positive microglia in the brains of Tg-APP/PS1 mice and humans with AD. Interestingly, in samples obtained from the former, SRCL-IR levels were low in astrocytes that were Aβ-negative. Thus, SRCL may be important in activated glial cell function in situations of neurodegeneration such as occur in AD.

We showed that SRCL-IR was not present in endothelial cells of the healthy adult brain (mouse or human), which contrasts with findings for mouse cardiac endothelial cells (Ohtani et al., 2001). Although the reason for this difference is not clear, tissue and age differences or differences in reagents used could explain this discrepancy. In contrast to healthy brains, we observed significant SRCL-IR in endothelial cells closely associated with cerebral amyloid angiopathy (CAA) in patients with AD, suggesting a role for SRCL in Aβ-loaded (stressed) endothelial cells. In addition, we found strong SRCL-IR in smooth muscle cells and MATO cells closely associated with CAA. Our ability to observe colocalization of Aβ and SRCL in intracellular compartments of vascular cells suggests that SRCL may function in internalization/clearance of Aβ-peptide. Strong binding of $fA\beta_{1-42}$ to CHO-K1 cells that expressed SRCL further supports this hypothesis.

The mechanisms by which SRCL expression is controlled are not well understood. However, as Aβ activates a variety of transcriptional signals, such as AP-1, NF-κB and cAMP responsive element-binding protein (CREB) at Ser133, and such signals have been proposed as a mechanism for Aβ-induced changes in gene expression (McDonald et al., 1998; Yin et al., 2002; Kim et al., 2003) and because we found corresponding consensus sequences for AP-1 and NF-κB in the promoter and 5′ UTR of *SRCL*, it is possible that some of these signals in glial and vascular cells could be involved in the mechanisms regulating *SRCL* expression.

The scavenger receptors A, BI (SR-A, SR-BI), and CD36, a complex involving CD36, α(6)β(1)-integrin as well as CD47, and heparan sulfate proteoglycans on glial cells have been reported to bind Aβ. A role for these microglial scavenger receptors in the Aβ-induced activation of inflammatory responses has been proposed. However, the role of the receptors in the clearance of Aβ is not yet well understood (Verdier and Penke, 2004; Ricciarelli et al., 2004). Even in the case of suggested scavenger receptors, their contribution has been considered to be partial. For example, although microglial or astroglial binding or internalization of $fA\beta_{1-42}$ peptide mediated through other receptors has been suggested for several SR family members, including SR-AI, SR-BI, CD36, and MARCO, no single receptor has been found to be essential. Indeed, deletion of SR-A by genetic knock-out did not increase amyloid plaque formation or neurodegeneration in transgenic mice expressing human amyloid protein precursors (Huang et al., 1999), suggesting the presence of alternative receptors for glial-mediated Aβ clearance.

The vascular system also may play a role in Aβ clearance. It has been suggested that LDL receptor-related protein-1 (LRP-1), a SR that binds various ligands including apoE, α2-macroglobulin, and APP, may function in Aβ vascular transport in young mice. When $A\beta_{1-40}$ was intracerebrally administered at high concentrations, LRP-1 facilitated $A\beta_{1-40}$ transport across the blood brain barrier (BBB) into the plasma. However, when given at lower concentrations of $A\beta_{1-40}$, anti-LRP antibody did not affect the clearance of $A\beta_{1-40}$ (Shibata et al., 2000). Thus Shibata et al. suggested the presence of an alternative, highly sensitive BBB transport mechanism, in addition to LRP-1. The molecular nature of this putative second transport system is not known. Some receptors have been proposed, e.g., the receptor for advanced glycosylation end-products (RAGE) and LRP-2; but they are unlikely to be involved in the rapid clearance of Aβ from the brain, and responsible receptor has yet to be found (Shibata et al., 2000). Considering such findings, our present data suggest SRCL to be the additional receptor responsible for vascular clearance of Aβ. The fact must be considered that increased amounts of fAβ itself increases Aβ deposition in vessel walls and can importantly affect in CAA, presumably due to the Aβ-dependent regulation of the receptors responsible for Aβ clearance. As most candidate SRs, such as CD36, are indeed downregulated in the adult (aged) brain even in the healthy condition or in the AD-affected brain, they thus may not play significant roles in the late stage of AD (Husemann et al., 2002). It seems likely that upregulated SRCL in association with Aβ-plaque and CAA could play an important role in Aβ clearance in an Aβ dose-dependent manner. Other mechanisms, such as those causing decreased vessel elasticity, have been suggested to reduce the efficiency of Aβ clearance. For example, ablation of the nucleus basalis in the rabbit, the source of cholinergic innervation of blood vessels in the brain, results in CAA (Roher et al., 2000), suggesting that disturbance of blood vessel tone and pulsations could be a factor in deposition of Aβ in artery walls. Loss of elasticity in aging human cerebral arteries with progressive arteriosclerosis (Perry et al., 1998; Kalaria, 2001) or cessation of pulsations with focal thromboembolic occlusion (Weller et al., 2002) might play a role in impeding drainage of Aβ and in pathogenesis of CAA

(Weller et al., 2002). As it has been suggested that SRs are involved in attenuation of arteriosclerosis due to their capability to bind Oxy-LDL (Rigotti, 2000), and because SRCL has the ability to bind Oxy-LDL, we may postulate that upregulated SRCL on vascular cells may play a role in attenuating loss of elasticity of brain vessels in aged patients with AD, thereby indirectly improving the clearance of Aβ.

Based on all data taken together, we propose that SRCL on glial or cerebral vascular/perivascular cells functions as a physiological receptor, upregulated by Aβ and pivotally facilitating the clearance of substances such as Aβ and LDL in AD-affected brain tissues, thus attenuating disease progression. We are currently developing SRCL-null mice, and the generation and analysis of triple transgenic offspring of SRCL-null and Tg-APP/PS1 mice may clarify the contribution of SRCL and allow us to devise new approaches targeting SRCL for the clearance of Aβ in AD.

In summary, this is the first description of the upregulation and possible role of SRCL in the binding or clearance of Aβ by glial and vascular/perivascular cells associated with AD. Our findings provide a new insight into the pathophysiology of AD and suggest future SRCL-based therapeutic interventions against Aβ-mediated pathogenesis in AD.

ACKNOWLEDGMENTS

We are grateful to Dr. Checler for kindly providing anti-Aβ antibodies (rabbit anti-Aβ40 (FCA3340) and anti-Aβ42 (FCA3542) antibodies). We are also grateful to Dr. Kadoyama for the help with astrocyte cultures and Dr. Kanzaki for the generation of CHO-K1 cells stably expressing mSRCL-Flag. This work was supported in part by research grants from COE to T.N., and by grants from the Ministry of Education, Science, Technology, Sports and Culture of Japan and Ministry of Health and Welfare of Japan to T.N. and H.F.

REFERENCES

Alarcon R, Fuenzalida C, Santibanez M, von Bernhardi R. 2005. Expression of scavenger receptors in glial cells. Comparing the adhesion of astrocytes and microglia from neonatal rats to surface-bound beta-amyloid. J Biol Chem 280:30406–30415.

Bard F, Cannon C, Barbour R, Burke RL, Games D, Grajeda H, Guido T, Hu K, Huang J, Johnson-Wood K, Khan K, Kholodenko D, Lee M, Lieberburg I, Motter R, Nguyen M, Soriano F, Vasquez N, Weiss K, Welch B, Seubert P, Schenk D, Yednock T. 2000. Peripherally administered antibodies against amyloid beta-peptide enter the central nervous system and reduce pathology in a mouse model of Alzheimer disease. Nat Med 6:916–919.

DeMattos RB, Bales KR, Cummins DJ, Paul SM, Holtzman DM. 2002. Brain to plasma amyloid-beta efflux: a measure of brain amyloid burden in a mouse model of Alzheimer's disease. Science 295:2264–2267.

El Khoury JB, Moore KJ, Means TK, Leung J, Terada K, Toft M, Freeman MW, Luster AD. 2003. CD36 mediates the innate host response to beta-amyloid. J Exp Med 197:1657–1666.

Funakoshi H, Okuno S, Fujisawa H. 1991. Different effects on activity caused by phosphorylation of tyrosine hydroxylase at serine 40 by three multifunctional protein kinases. J Biol Chem 266:15614–15620.

Funakoshi H, Yonemasu T, Nakano T, Matumoto K, Nakamura T. 2002. Identification of Gas6, a putative ligand for Sky and Axl receptor tyrosine kinases, as a novel neurotrophic factor for hippocampal neurons. J Neurosci Res 68:150–160.

Guenette SY. 2003a. Astrocytes: a cellular player in Abeta clearance and degradation. Trends Mol Med 9:279–280.

Guenette SY. 2003b. Mechanisms of Abeta clearance and catabolism. Neuromolecular Med 4:147–160.

Hsiao K, Chapman P, Nilsen S, Eckman C, Harigaya Y, Younkin S, Yang F, Cole G. 1996. Correlative memory deficits, Abeta elevation, and amyloid plaques in transgenic mice. Science 274:99–102.

Huang F, Buttini M, Wyss-Coray T, McConlogue L, Kodama T, Pitas RE, Mucke L. 1999. Elimination of the class A scavenger receptor does not affect amyloid plaque formation or neurodegeneration in transgenic mice expressing human amyloid protein precursors. Am J Pathol 155: 1741–1747.

Husemann J, Loike JD, Anankov R, Febbraio M, Silverstein SC. 2002. Scavenger receptors in neurobiology and microglia and other cells of the nervous system. Glia 40:195–205.

Kakimura J, Kitamura Y, Takata K, Umeki M, Suzuki S, Shibagaki K, Taniguchi T, Nomura Y, Gebicke-Haerter PJ, Smith MA, Perry G, Shimohama S. 2002. Microglial activation and amyloid-beta clearance induced by exogenous heat-shock proteins. FASEB J 16:601–603.

Kalaria RN. 2001. Advances in molecular genetics and pathology of cerebrovascular disorders. Trends Neurosci 24:392–400.

Kim JY, Kim H, Lee SG, Choi BH, Kim YH, Huh PW, Lee KH, Han H, Rha HK. 2003. Amyloid beta peptide (Abeta42) activates PLC-delta1 promoter through the NF-kappaB binding site. Biochem Biophys Res Commun 310:904–909.

Kodama T, Freeman M, Rohrer L, Zabrecky J, Matsudaira P, Krieger M. 1990. Type I macrophage scavenger receptor contains alpha-helical and collagen-like coiled coils. Nature 343:531–535.

Koistinaho M, Lin S, Wu X, Esterman M, Koger D, Hanson J, Higgs R, Liu F, Malkani S, Bales KR, Paul SM. 2004. Apolipoprotein E promotes astrocyte colocalization and degradation of deposited amyloid-beta peptides. Nat Med 10:719–726.

Matsuoka Y, Saito M, LaFrancois J, Gaynor K, Olm V, Wang L, Casey E, Lu Y, Shiratori C, Lemere C, Duff K. 2003. Novel therapeutic approach for the treatment of Alzheimer's disease by peripheral administration of agents with an affinity to beta-amyloid. J Neurosci 23:29–33.

McDonald DR, Bamberger ME, Combs CK, Landreth GE. 1998. beta-Amyloid fibrils activate parallel mitogen-activated protein kinase pathways in microglia and THP1 monocytes. J Neurosci 18:4451–4460.

Murphy JE, Tedbury PR, Homer-Vanniasinkam S, Walker JH, Ponnambalam S. 2005. Biochemistry and cell biology of mammalian scavenger receptors. Atherosclerosis 182:1–15.

Nakamura K, Funakoshi H, Miyamoto K, Tokunaga F, Nakamura T. 2001a. Molecular cloning and functional characterization of a human scavenger receptor with C-type lectin (SRCL), a novel member of a scavenger receptor family. Biochem Biophys Res Commun 280:1028–1035.

Nakamura K, Funakoshi H, Tokunaga F, Nakamura T. 2001b. Molecular cloning of a mouse scavenger receptor with C-type lectin (SRCL)(1), a novel member of the scavenger receptor family. Biochim Biophys Acta 1522:53–58.

Nakano Y, Kondoh G, Kudo T, Imaizumi K, Kato M, Miyazaki JI, Tohyama M, Takeda J, Takeda M. 1999. Accumulation of murine amyloidbeta42 in a gene-dosage-dependent manner in PS1 'knock-in' mice. Eur J Neurosci 11:2577–2581.

Naveilhan P, Neveu I, Baudet C, Funakoshi H, Wion D, Brachet P, Metsis M. 1996. 1, 25-Dihydroxyvitamin D3 regulates the expression of the low-affinity neurotrophin receptor. Brain Res Mol Brain Res 41:259–268.

Nicoll JA, Weller RO. 2003. A new role for astrocytes: beta-amyloid homeostasis and degradation. Trends Mol Med 9:281–282.

Ohtani K, Suzuki Y, Eda S, Kawai T, Kase T, Keshi H, Sakai Y, Fukuoh A, Sakamoto T, Itabe H, Suzutani T, Ogasawara M, Yoshida I, Wakamiya N. 2001. The membrane-type collectin CL-P1 is a scavenger endothelial cells. J Biol Chem 276:44222–44228.

Paresce DM, Ghosh RN, Maxfield FR. 1996. Microglial cells internalize aggregates of the Alzheimer's disease amyloid beta-protein via a scavenger receptor. Neuron 17:553–565.

Perry G, Smith MA, McCann CE, Siedlak SL, Jones PK, Friedland RP. 1998. Cerebrovascular muscle atrophy is a feature of Alzheimer's disease. Brain Res 791:63–66.

Ricciarelli R, D'Abramo C, Zingg JM, Giliberto L, Markesbery W, Azzi A, Marinari UM, Pronzato MA, Tabaton M. 2004. CD36 overexpression in human brain correlates with beta-amyloid deposition but not with Alzheimer's disease. Free Radic Biol Med 36:1018–1024.

Rigotti A. 2000. Scavenger receptors and atherosclerosis. Biol Res 33: 97–103.

Roher AE, Kuo YM, Potter PE, Emmerling MR, Durham RA, Walker DG, Sue LI, Honer WG, Beach TG. 2000. Cortical cholinergic denervation elicits vascular A beta deposition. Ann NY Acad Sci 903:366–373.

Shibata M, Yamada S, Kumar SR, Calero M, Bading J, Frangione B, Holtzman DM, Miller CA, Strickland DK, Ghiso J, Zlokovic BV. 2000. Clearance of Alzheimer's amyloid-ss(1-40) peptide from brain by LDL receptor-related protein-1 at the blood-brain barrier. J Clin Invest 106:1489–1499.

Tanzi RE, Bertram L. 2005. Twenty years of the Alzheimer's disease amyloid hypothesis: a genetic perspective. Cell 120:545–555.

Tanzi RE, Moir RD, Wagner SL. 2004. Clearance of Alzheimer's Abeta peptide: the many roads to perdition. Neuron 43:605–608.

Verdier Y, Penke B. 2004. Binding sites of amyloid beta-peptide in cell plasma membrane and implications for Alzheimer's disease. Curr Protein Pept Sci 5:19–31.

Weller RO, Yow HY, Preston SD, Mazanti I, Nicoll JA. 2002. Cerebrovascular disease is a major factor in the Abeta from the aging human brain: implications for disease. Ann NY Acad Sci 977:162–168.

Wyss-Coray T, Lin C, Yan F, Yu GQ, Rohde M, McConlogue L, Masliah E, Mucke L. 2001. TGF-beta1 promotes microglial amyloid-beta clearance and reduces plaque burden in transgenic mice. Nat Med 7:612–618.

Wyss-Coray T, Loike JD, Brionne TC, Lu E, Anankov R, Yan F, Silverstein SC, Husemann J. 2003. Adult mouse astrocytes degrade amyloid-beta in vitro and in situ. Nat Med 9:453–457.

Yin KJ, Lee JM, Chen SD, Xu J, Hsu CY. 2002. Amyloid-beta induces Smac release via AP-1/Bim activation in cerebral endothelial cells. J Neurosci 22:9764–9770.

Zlokovic BV. 2004. Clearing amyloid through the blood-brain barrier. J Neurochem 89:807–811.

Available online at www.sciencedirect.com
SCIENCE DIRECT
Biochemical and Biophysical Research Communications 344 (2006) 525–530
BBRC
www.elsevier.com/locate/ybbrc

Altered localization of amyloid precursor protein under endoplasmic reticulum stress

Takashi Kudo [a,*], Masayo Okumura [b], Kazunori Imaizumi [c], Wataru Araki [d], Takashi Morihara [a], Hitoshi Tanimukai [a], Eiichiro Kamagata [a], Nobuhiko Tabuchi [a], Ryo Kimura [a], Daisuke Kanayama [a], Akio Fukumori [a], Shinji Tagami [a], Masayasu Okochi [a], Mikiko Kubo [a], Hisashi Tanii [e], Masaya Tohyama [f], Takeshi Tabira [g], Masatoshi Takeda [a]

[a] *Division of Psychiatry, Course of Internal Medicine, Osaka University Graduate School of Medicine, Osaka, Japan*
[b] *Institute for Oral Science, Matsumoto Dental University, Nagano, Japan*
[c] *Division of Molecular and Cellular Biology, Department of Anatomy, Miyazaki Medical College, Miyazaki, Japan*
[d] *Department of Demyelinating Disease and Aging, National Institute of Neuroscience, Tokyo, Japan*
[e] *Department of Psychiatry, Mie University Graduate School of Medicine, Mie, Japan*
[f] *Department of Anatomy and Neuroscience, Osaka University Graduate School of Medicine, Osaka, Japan*
[g] *National Institute for Longevity Sciences, Aichi, Japan*

Received 9 March 2006
Available online 5 April 2006

Abstract

Recent reports have shown that the endoplasmic reticulum (ER) stress is relevant to the pathogenesis of Alzheimer disease. Following the amyloid cascade hypothesis, we therefore attempted to investigate the effects of ER stress on amyloid-β peptide (Aβ) generation. In this study, we found that ER stress altered the localization of amyloid precursor protein (APP) from late compartments to early compartments of the secretory pathway, and decreased the level of Aβ 40 and Aβ 42 release by β- and γ-cutting. Transient transfection with BiP/GRP78 also caused a shift of APP and a reduction in Aβ secretion. It was revealed that the ER stress response facilitated binding of BiP/GRP78 to APP, thereby causing it to be retained in the early compartments apart from a location suitable for the cleavages of Aβ. These findings suggest that induction of BiP/GRP78 during ER stress may be one of the regulatory mechanisms of Aβ generation.

Keywords: Alzheimer's disease; Endoplasmic reticulum; Amyloid-β peptide; Amyloid precursor protein; BiP/GRP78

The first genetic mutations shown to be involved in Alzheimer disease (AD) were discovered in the amyloid precursor protein (APP) gene. These mutations promote the generation of amyloid-β peptide (Aβ) as a sticky molecule that forms senile plaques in the AD brain. Other AD-causing mutations were subsequently identified in presenilin-1 and -2 (PS1 and PS2, respectively) and shown to enhance the processing of APP into amyloidogenic Aβ. Following these discoveries, many reports have shown that cerebral Aβ accumulation primarily influences the AD brain and subsequent steps in the disease process, including neurofibrillary tangles of tau proteins [1]. Therefore, the amyloid cascade hypothesis has led many researchers to investigate Aβ generation. Recent studies have revealed that APP is first cleaved by a β-secretase, BACE1, at the N-terminus of Aβ, followed by an intramembranous second cleavage at the C-terminus of Aβ by a γ-secretase. The γ-secretase activity is controlled by PS1 complexes consisting of heteromeric molecules, including nicastrin, PEN-2, and APH-1 [2]. Although PS1 is mainly located in the endoplasmic reticulum (ER), γ-complexes have also been identified in the plasma membrane and endosomes where they execute γ-cleavage [3,4].

Recent reports have showed that the endoplasmic reticulum (ER) stress is relevant to the pathogenesis of AD.

* Corresponding author. Fax: +81 6 6879 3059.
E-mail address: kudo@psy.med.osaka-u.ac.jp (T. Kudo).

0006-291X/$ - see front matter © 2006 Elsevier Inc. All rights reserved.
doi:10.1016/j.bbrc.2006.03.173

Nakagawa et al. [5] reported that caspase-12, which causes an ER-mediated apoptosis due to ER stress, contributes to Aβ neurotoxicity. It has been also reported that mutations in PS1 and PS2 perturb ER calcium homeostasis causing ER stress [6]. These findings led us to investigate the relationship between ER stress and Aβ generation, i.e., APP processing. In the present study, we show that ER stress affects APP processing by inducing a molecular chaperone.

Materials and methods

Cell culture and cell lines. SH-SY5Y human neuroblastoma cells were stably transfected with Swedish mutant APP670/671 (SY5Y/swAPP). The appearance and growth rate of SY5Y/swAPP cells were similar to those of mock vector-transfected cells. HEK293 cells were stably transfected with V5-tagged nicastrin (293/Nct-V5). Primary fibroblasts were obtained from PS1/PS2$^{-/-}$ mice embryos on embryonic day 14.5. All cells were cultured in Dulbecco's modified Eagle's medium (DMEM; Gibco, Grand Island, NY, USA), supplemented with either 10% fetal calf serum (FCS) for SH-SY5Y cells or 20% FCS for HEK293 cells and embryonic fibroblasts.

Antibodies. An anti-Aβ42 monoclonal antibody, KM10, was obtained by serial immunization of mice with the synthetic peptide MVGGVVIA. An anti-PS1 antibody was raised against a synthetic peptide corresponding to residues 1–14 of human PS1. An anti-V5 antibody (Invitrogen, Carlsbad, CA, USA) was used for BN-PAGE. An anti-APP antibody (Chemicon, Temecula, CA, USA) was used for immunoblotting. Anti-Aβ antibodies, 4G8 and 6E10 (Signet Pathology Systems Inc., Dedham, MA, USA), were used for immunoprecipitation and immunoblotting of Aβ, respectively. Anti-calnexin and anti-Lys-Asp-Glu-Leu (KDEL) antibodies recognizing BiP/GRP78 (Stressgen, Victoria, BC, Canada) were used for immunoprecipitation and immunoblotting as ER markers. An anti-GM130 antibody (BD Biosciences, Mississauga, ON, Canada) was used for immunoblotting as a *cis*-Golgi marker. An anti-β-actin monoclonal antibody was purchased from Chemicon.

ER stress. At 2 days before stimulation by ER stressors, 3×10^5 SY5Y/swAPP cells were plated in 10-cm diameter dishes, and then given fresh culture medium on the following day. In all ER stress response experiments, we used culture dishes showing 70–80% confluency to avoid stress induced by overgrowth. On the day of stimulation, the cells were placed in fresh medium for at least 60 min before treatment to create similar conditions in each dish. Appropriate doses of thapsigargin and tunicamycin (Sigma, St. Louis, MO, USA) were applied for 24 h as ER stress inducers. Control dishes were treated by simply changing the culture media.

Immunoprecipitation and immunoblotting. Following centrifugation of 10-ml aliquots of SY5Y/swAPP media at 2500*g* for 5 min, 15 μl of protein G–Sepharose (Gibco), 5 μl of 4G8 (anti-Aβ antibody), 10 μl of 1 M Tris–HCl, pH 7.8, 8 μl of 0.5 M EDTA, and 8 μl protease inhibitor cocktail (Sigma) were added to 8 ml of each supernatant. After allowing the immunoreactions to proceed for 18 h, the beads were washed four times with RIPA buffer, boiled with sample buffer for 5 min, and applied to a 15/25 PAG Mini gel (Daiichi, Tokyo, Japan). Following SDS/PAGE, the separated proteins were transferred to a nitrocellulose membrane and probed using 6E10 (anti-Aβ antibody).

ELISA. ELISA kits for Aβ 40 and Aβ 42 were purchased from Biosource International (Camarillo, CA, USA) and used according to the manufacturer's instructions. All ELISAs were carried out in duplicate.

Blue native gel electrophoresis (BN-PAGE). At 1 day prior to analysis, 5–13.5% polyacrylamide gels for BN-PAGE were prepared. Following cell lysis in 1% CHAPSO (Calbiochem, San Diego, CA, USA), 500 mM e-aminocaproic acid, 20 mM Hepes, pH 7.4, 2 mM EDTA, and 10% glycerol, the lysates were incubated on ice for 60 min and then centrifuged at 100,000*g* for 60 min. The supernatants were subjected to BN-PAGE [7]. The gels were subsequently soaked in 0.1% SDS for 10 min and electrotransferred to polyvinylidene difluoride membranes in a standard buffer containing 0.01% SDS.

γ-Secretase assay. Membrane isolation from SY5Y/swAPP cells was carried out as previously described [8]. Briefly, cell lysates were suspended in buffer A (20 mM Hepes, pH 7.5, 50 mM KCl, 2 mM EGTA, and protease inhibitor mixture), homogenized using a Dounce homogenizer, and washed once with buffer A by centrifugation at 800*g* for 10 min. The resulting supernatants were pooled and centrifuged at 100,000*g* for 1 h. The membranes were resuspended in buffer B (20 mM Hepes, pH 7.0, 150 mM KCl, 2 mM EGTA, 1% CHAPSO, and protease inhibitor mixture), solubilized at 4 °C for 1 h, and collected by centrifugation at 100,000*g* for 1 h. For measurement of the γ-secretase activity, the solubilized membranes were incubated at 37 °C in 150 μl of assay buffer (50 mM Tris–HCl, pH 6.8, 2 mM EDTA, and 0.25% CHAPSO) and then incubated with 8 μM of the fluorogenic γ-secretase substrate Nma-GGVVIATVK[DNP]-rrr-NH_2 [8] at 37 °C overnight. After a subsequent incubation with 5 μM of the γ-secretase inhibitor L685.458 (Bachem, Bubendorf, Switzerland) or appropriate doses of thapsigargin or tunicamycin, the reaction mixtures were centrifuged at 16,100*g* for 15 min, transferred to a 96-well plate, and measured in a plate reader using an excitation wavelength of 355 nm and an emission wavelength of 440 nm.

Subcellular fractionation. SY5Y/swAPP cells in 14-cm diameter dishes were harvested in 1.6 ml of ice-cold homogenization buffer (10 mM triethanolamine, 10 mM acetic acid, 250 mM sucrose, 1 mM EDTA, 1 mM DTT, and protease inhibitor cocktail) and homogenized by 10 passages through a 25 G needle. Post-nuclear supernatants were obtained by centrifugation at 9500*g* for 10 min at 4 °C using a Sorvall SS-34 rotor and fractionated by centrifugation in a Nycodenz gradient as described previously [9,10]. Briefly, a step gradient was created in Beckman SW41 centrifuge tubes by loading (from top to bottom) 2.5 ml aliquots of 10%, 14.66%, 19.33%, and 24% Nycodenz solutions in saline buffer. The individual solutions were prepared from a 27.6% Nycodenz stock solution and 0.75% NaCl (both in 10 mM Tris–HCl, pH 7.4, 3 mM KCl, 1 mM EDTA, and 0.02% NaN_3). The tubes were sealed with Parafilm, placed horizontally at room temperature for 45 min and then centrifuged at 37,000 rpm for 4 h at 15 °C using a SW41 rotor to create nonlinear gradients. Next, 800 μl aliquots of the post-nuclear supernatants were layered on top of the gradients and fractionated by centrifugation at 37,000 rpm for 1.5 h at 15 °C. After the centrifugation, 10 fractions (1 ml each) were collected from the top of each tube. The subcellular fractions were characterized by probing with antibodies against specific marker proteins of various subcellular compartments, such as calnexin and GM130.

Incorporation immunoprecipitation. SY5Y/swAPP cells were extracted with 1% Nonidet P-40 lysis buffer, followed by immunoprecipitation using anti-APP antibody 22C11 or anti-KDEL antibody (recognizing BiP/GRP78) and protein G–Sepharose beads. After washing, Western blot analyses were performed with anti-APP or anti-KDEL antibodies.

Transfection with BiP/GRP78. A wild-type hamster BiP/GRP78 expression plasmid was kindly provided by L. Hendershot (St. Jude Children's Research Hospital, Memphis, TN, USA). Hamster BiP/GRP78 shows >99% identity to human BiP/GRP78. SY5Y/swAPP cells were transfected using Lipofectamine 2000 (Invitrogen) according to the manufacturer's instructions.

Statistical analysis. The results are presented as means ± SD. Significant differences among groups were determined using the unpaired Student's *t* test. For all analyses, $p < 0.05$ was considered statistically significant.

Results and discussion

SY5Y/swAPP cells, which were permanently transfected with Swedish mutant APP, at 70–80% confluence were placed in fresh culture medium for more than 60 min before treatment with the ER stressors thapsigargin and tunicamycin at appropriate doses for 24 h. Immunoprecipitation and immunoblotting revealed that thapsigargin treatment decreased the secreted total Aβ in media of SY5Y/swAPP cells in a dose-dependent manner

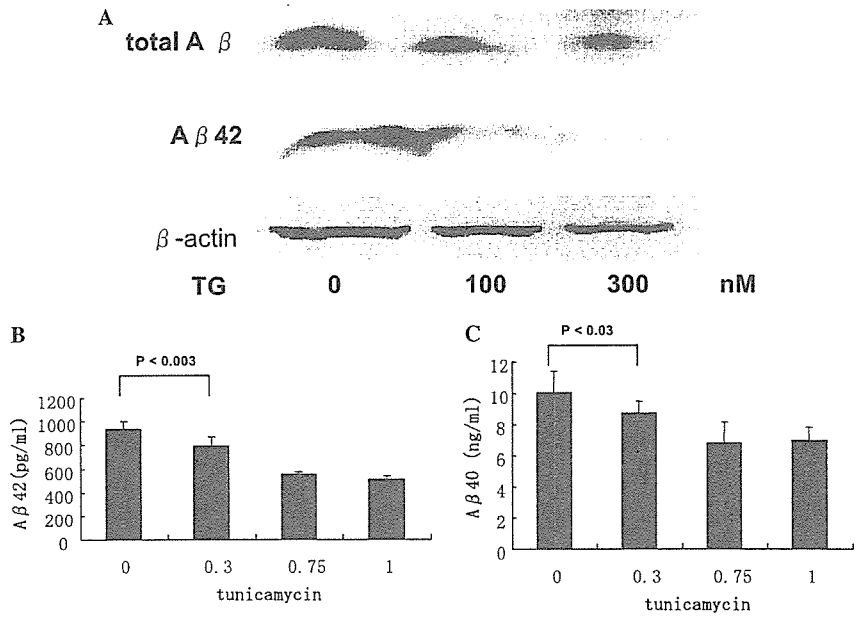

Fig. 1. Reduced Aβ generation following ER stress. (A) SY5Y/swAPP cells were treated with thapsigargin (TG; 0, 100 or 300 nM) for 24 h, and the media were collected and immunoprecipitated with anti-Aβ antibodies (4G8 for total Aβ; KM10 for Aβ 42) and protein G–Sepharose beads. Immunoblotting was probed another Aβ antibody (6E10). (B) The levels of Aβ 42 secreted from SY5Y/swAPP cells treated with 0.3, 0.75 or 1.0 μg/ml tunicamycin were measured by ELISA. Data are expressed as means ± SD ($n = 6$). (C) The levels of Aβ 40 secreted by SY5Y/swAPP cells treated with 0.3, 0.75 or 1.0 μg/ml tunicamycin were measured by ELISA. Data are expressed as means ± SD ($n = 6$).

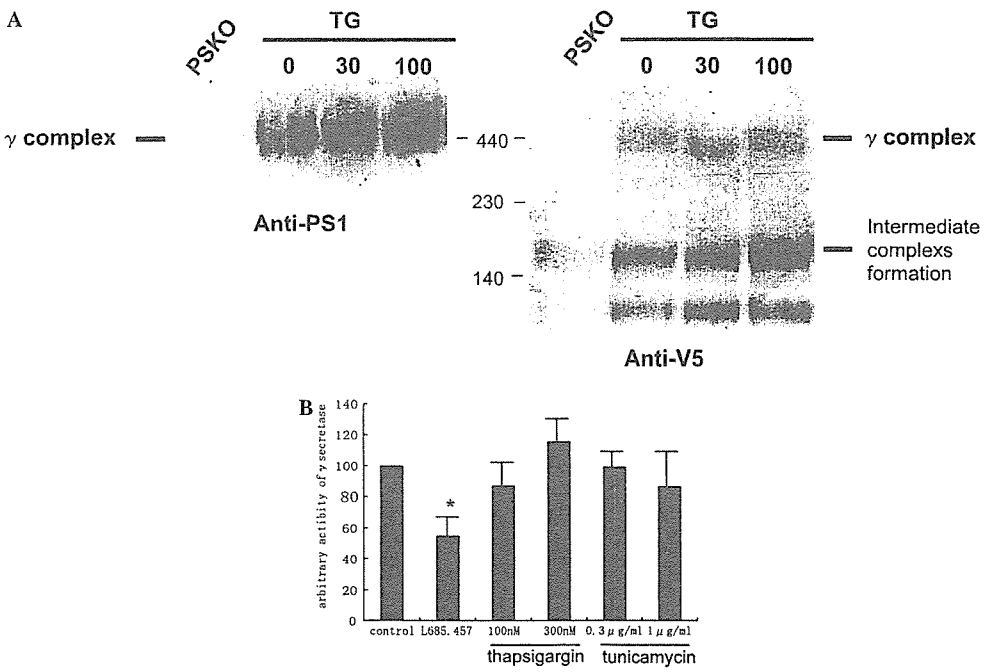

Fig. 2. γ-Secretase activity under ER stress. (A) γ-Complexes under ER stress. 293/Nct-V5 cells treated with thapsigargin (TG) were lysed with 1% CHAPSO, 500 mM e-aminocaproic acid, 20 mM Hepes, pH 7.4, 2 mM EDTA, and 10% glycerol and then centrifuged at 100,000g for 60 min. The supernatants were subjected to BN-PAGE. Immunostaining was probed with anti-PS1 antibodies and anti-V5 antibodies. PSKO: PS1/PS2$^{-/-}$. (B) Solubilized membrane preparations from SY5Y/swAPP cells were incubated with 8 μM of the fluorogenic γ-secretase substrate Nma-GGVVIATVK[DNP]-rrr-NH_2 at 37 °C overnight. After incubation with 5 μM of the γ-secretase inhibitor L685.458 or appropriate doses of thapsigargin or tunicamycin, the reactions were centrifuged at 16,100g for 15 min, transferred to a 96-well plate and measured in a plate reader using an excitation wavelength of 355 nm and an emission wavelength of 440 nm. The values are shown as the percent difference from the control ±SD ($n = 5$). *$p < 0.05$.

(Fig. 1A). The level of Aβ 42 was markedly decreased in the presence of 100 nM thapsigargin (Fig. 1A). The level of intracellular β-actin as an internal control remained unchanged under ER stress, suggesting that these levels of ER stress do not cause apparent cell death. ELISA analyses further demonstrated significant reductions in the Aβ 42 and Aβ 40 levels in media from SY5Y/swAPP cells treated with 0.3, 0.75, and 1.0 μg/ml tunicamycin (Figs. 1B and C). These data suggest that ER stress may suppress Aβ generation.

Recent studies have shown that Aβ generation requires the actions of high molecular mass complexes consisting of PS1, nicastrin, Aph-1, and Pen-2 with γ-secretase activity [11]. 293/Nct-V5 cells, which were transfected with V5-tagged nicastrin, were stressed using appropriate doses of thapsigargin for 24 h, lysed and subjected to BN-PAGE. Immunostaining using anti-PS1 and anti-V5 antibodies revealed that the γ-complexes were unchanged after ER stress (Fig. 2A). Intermediate complexes formation, thought to be immature nicastrin and Aph-1 [12], also remained unchanged after ER stress. Since PS1/PS2$^{-/-}$ mouse (PSKO) embryonic fibroblasts do not have PS1, they do not have any γ-complexes (Fig. 2A). Using a fluorogenic synthetic polypeptide substrate to measure the γ-secretase activity, the doses of the ER stressors thapsigargin and tunicamycin that reduced Aβ production were found to have little influence on the enzyme activity, compared with the conventional γ-secretase inhibitor L685.458 (Fig. 2B). These data indicate that γ-complexes may be assembled and γ-secretase activity may be preserved under ER stress.

Subcellular compartments of SY5Y/swAPP cells were fractionated using a Nycodenz gradient, and each fraction was probed with antibodies against specific marker proteins by immunoblotting analysis. Two distinct subcellular compartments, namely the ER and Golgi, were separated. Fractions 1–5 were designated as belonging to the ER as they possessed calnexin, whereas fractions 8–10 were designated as belonging to the *cis*-Golgi as they showed GM 130 positivity (Fig. 3). Since the bottom fractions from the Nycodenz gradient were assumed to be contaminated with late compartments and plasma membranes, these fractions should contain APP localized in the compartments. Under normal conditions, APP was mainly located in the *cis*-Golgi fractions. Small amounts of APP, especially immature forms, were also distributed in the ER fractions. On the other hand, APP became accumulated in the ER fractions in cells under ER stress in the presence of 1 μM thapsigargin (Fig. 3).

It is assumed that ER stress activates a retrograde transport to the ER from post-ER compartment to avoid the delivery of unfolded proteins. It has been reported that BiP/GRP78, a KDEL protein, binds to unfolded proteins and that a C-terminal KDEL sequence is recognized by the KDEL receptor in post-ER compartments, leading to sorting into COPI vesicles for retrograde transport [13]. Therefore, we hypothesized that APP would bind to BiP/GRP78 under ER stress and undergo retrograde transport. Co-immunoprecipitation experiments using 22C11 and anti-KDEL antibodies revealed that BiP/GRP78 was bound to APP, and that the interaction was prominent under ER stress in the presence of 1 μM thapsigargin. Most of the APP molecules bound to BiP/GRP78 were immature forms, suggesting that BiP/GRP78 is prone to catching immature and unfolded APP (Fig. 4).

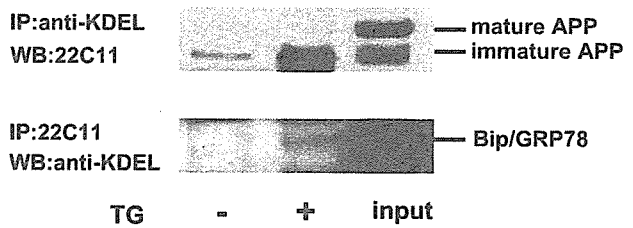

Fig. 4. BiP/GRP78 binding to APP under ER stress. SY5Y/swAPP cells treated with 1 μM thapsigargin (TG) for 24 h were extracted with 1% Nonidet P-40 lysis buffer for immunoprecipitation (IP) with anti-APP or anti-KDEL antibodies (recognizing BiP/GRP78) and protein G–Sepharose beads. After washing, Western blot (WB) analyses were mutually performed with anti-KDEL or anti-APP antibodies.

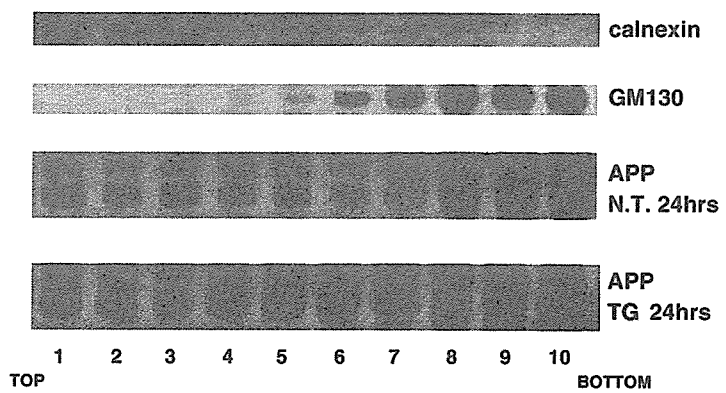

Fig. 3. Shift of APP under ER stress. SY5Y/swAPP cells treated with 1 μM thapsigargin for 24 h or left untreated (non-treated, N.T.) were lysed, fractionated through a Nycodenz gradient, and subjected to Western blot analysis to identify the distributions of calnexin (ER marker), GM130 (Golgi marker), and APP. TG, thapsigargin.

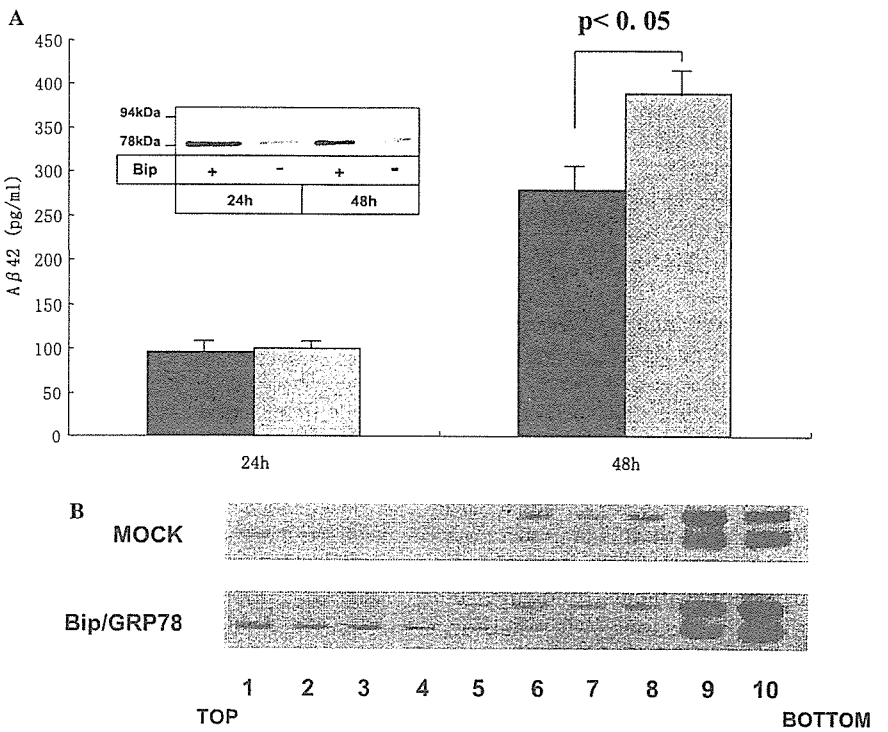

Fig. 5. Reduction in Aβ 42 secretion following transient transfection with a BiP/GRP78 construct. (A) SY5Y/swAPP cells were transiently transfected with a BiP/GRP78 construct and the concentrations of Aβ 42 in the conditioned media at 24 or 72 h after transfection were determined by ELISA. Black bars, BiP/GRP78 transfection; grey bars, mock vector transfection. Inset, Western blotting with an anti-KDEL antibody. Data are expressed as means ± SD ($n = 5$). (B) SY5Y/swAPP cells transfected with a BiP/GRP78 construct or mock vector were lysed, and fractionated through a Nycodenz step gradient.

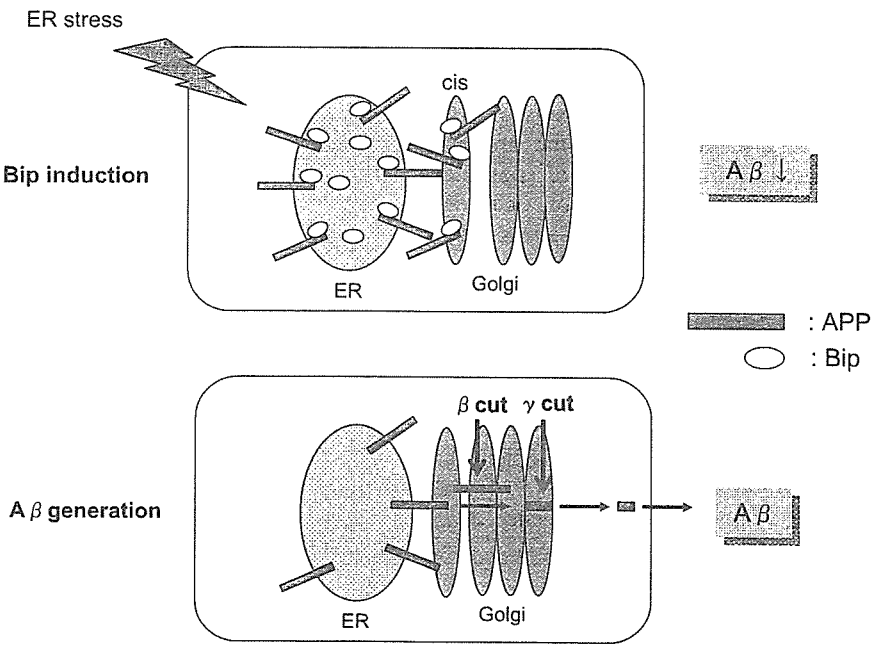

Fig. 6. Altered localization of APP as a result of ER stress. ER stress induces the ER chaperone BiP/GRP78 which binds to APP. APP bound with BiP/GRP78 is retained in the ER because the KDEL sequence of BiP/GRP78 is responsible for its recognition and retrieval from post-ER compartments. Since the β/γ-secretase activity itself is thought to be located in a distal compartment to the ER, ER stress may separate APP from a location suitable for β/γ-secretase cleavage.

To confirm that the induction of BiP/GRP78 reduces Aβ generation, SY5Y/swAPP cells were transiently transfected with a BiP/GRP78 construct. ELISA analysis of Aβ in the conditioned medium demonstrated that the levels of secreted Aβ 40 (not shown) and Aβ 42 were reduced at 78 h after the transfection of BiP/GRP78 (Fig. 5A). Immunoblotting of the Nycodenz gradient fractions of SY5Y/swAPP cells transfected with BiP/GRP78 showed that the induction of BiP/GRP78 caused a shift in APP to the early compartments (Fig. 5B).

These findings suggest that interactions between BiP/GRP78 and immature forms of APP in the ER may prevent APP translocation to distal compartments under ER stress. Regarding the reason why the secretions of Aβ 40 and Aβ 42 were reduced after ER stress, BN-PAGE and γ-secretase assays indicated that the activity of γ-secretase itself may remain unaffected by ER stress. Since γ-secretase activity is thought to exist in the late secretory pathway, plasma membrane, and endosomes [3,4], the APP remaining in the early compartments following ER stress may not reach a location suitable for cutting, resulting in a reduction in Aβ generation (Fig. 6).

IRE1 is one of the transducers for ER stress inducing BiP/GRP78. We previously reported that the maturation of APP was deteriorated in dominant-negative ΔIRE1 cells, a deletion mutant that lacks the kinase and RNase L domains necessary for induction of BiP/GRP78 [14]. Accordingly, we investigated the relationship between ER stress and Aβ generation. The present data indicate that ER stress induces BiP/GRP78 to bind to APP, thereby causing APP to be retained in the early compartments and resulting in a reduction in Aβ generation because β/γ-secretase activity itself is thought to be located in a distal compartment to the ER (Fig. 6). We conclude that the induction of BiP/GRP78 by ER stress may be one of the regulatory mechanisms of Aβ generation. Previously, we also verified that the protein levels of BiP/GRP78 decreased in the brains of sporadic AD as well as familial AD [15]. A combination of these findings and the present data suggest that ER stress may play an important role in AD pathology via the amyloid cascade.

Acknowledgments

This work was supported by a grant from the Ministry of Health, Labor, and Welfare (Mental Health Science), Japan, and a Grant-in-Aid for Scientific Research from the Ministry of Education, Culture, Sports, Science and Technology, Japan.

References

[1] J. Hardy, D.J. Selkoe, The amyloid hypothesis of Alzheimer's disease: progress and problems on the road to therapeutics, Science 297 (2002) 353–356.
[2] C. Haass, Take five BACE and the gamma-secretase quartet conduct Alzheimer's amyloid beta-peptide generation, EMBO J. 23 (2004) 483–488.
[3] P. Cupers, M. Bentahir, K. Craessaerts, I. Orlans, H. Vanderstichele, P. Saftig, B. De Strooper, W. Annaert, The discrepancy between presenilin subcellular localization and gamma-secretase processing of amyloid precursor protein, J. Cell Biol. 154 (2001) 731–740.
[4] W.G. Annaert, L. Levesque, K. Craessaerts, I. Dierinck, G. Snellings, D. Westaway, P.S. George-Hyslop, B. Cordell, P. Fraser, B. De Strooper, Presenilin 1 controls gamma-secretase processing of amyloid precursor protein in pre-golgi compartments of hippocampal neurons, J. Cell Biol. 147 (1999) 277–294.
[5] T. Nakagawa, H. Zhu, N. Morishima, E. Li, J. Xu, B.A. Yankner, J. Yuan, Caspase-12 mediated endoplasmic-reticulum-specific apoptosis and cytotoxicity by amyloid-beta, Nature 403 (2000) 98–103.
[6] M.P. Mattson, S.L. Chan, Dysregulation of cellular calcium homeostasis in Alzheimer's disease: bad genes and bad habits, J. Mol. Neurosci. 17 (2001) 205–224.
[7] H. Schagger, W.A. Cramer, G. von Jagow, Analysis of molecular masses and oligomeric states of protein complexes by blue native electrophoresis and isolation of membrane protein complexes by two-dimensional native electrophoresis, Anal. Biochem. 217 (1994) 220–230.
[8] M.R. Farmery, L.O. Tjernberg, S.E. Pursglove, A. Bergman, B. Winblad, J. Näslund, Partial purification and characterization of γ-secretase from post-mortem human brain, J. Biol. Chem. 278 (2003) 24277–24284.
[9] C. Hammond, A. Helenius, Quality control in the secretory pathway: retention of a misfolded viral membrane glycoprotein involves cycling between the ER, intermediate compartment, and Golgi apparatus, J. Cell Biol. 126 (1994) 41–52.
[10] D. Rickwood, T. Ford, J. Graham, Nycodenz: a new nonionic iodinated gradient medium, Anal. Biochem. 123 (1982) 23–31.
[11] B. De Strooper, Aph-1, Pen-2, and Nicastrin with Presenilin generate an active gamma-Secretase complex, Neuron 38 (2003) 9–12.
[12] M.J. LaVoie, P.C. Fraering, B.L. Ostaszewski, W. Ye, T. Kimberly, M.S. Wolfe, D.J. Selkoe, Assembly of the gamma-secretase complex involves early formation of an intermediate subcomplex of Aph-1 and nicastrin, J. Biol. Chem. 278 (2003) 37213–37222.
[13] K. Yamamoto, R. Fujii, Y. Toyofuku, T. Saito, H. Koseki, V.W. Hsu, T. Aoe, The KDEL receptor mediates a retrieval mechanism that contributes to quality control at the endoplasmic reticulum, EMBO J. 20 (2001) 3082–3091.
[14] N. Sato, K. Imaizumi, T. Manabe, M. Taguchi, J. Hitomi, T. Katayama, T. Yoneda, T. Morihara, Y. Yasuda, T. Takagi, T. Kudo, T. Tsuda, Y. Itoyama, T. Makifuchi, P.E. Fraser, P.St. George-Hyslop, M. Tohyama, Increased production of beta-amyloid and vulnerability to endoplasmic reticulum stress by an aberrant spliced form of presenilin 2, J. Biol. Chem. 276 (2001) 2108–2114.
[15] T. Katayama, K. Imaizumi, N. Sato, K. Miyoshi, T. Kudo, J. Hitomi, T. Morihara, T. Yoneda, F. Gomi, Y. Mori, Y. Nakano, J. Takeda, T. Tsuda, Y. Itoyama, O. Murayama, A. Takashima, P.St. George-Hyslop, M. Takada, M. Tohyama, Presenilin-1 mutations downregulate the signalling pathway of the unfolded-protein response, Nat. Cell Biol. 1 (1999) 479–485.

Presenilin-Dependent γ-Secretase on Plasma Membrane and Endosomes Is Functionally Distinct†

Akio Fukumori,‡,§ Masayasu Okochi,*,‡,§ Shinji Tagami,‡,§ Jingwei Jiang,§ Naohiro Itoh,§ Taisuke Nakayama,§ Kanta Yanagida,§ Yoshiko Ishizuka-Katsura,§ Takashi Morihara,§ Kojin Kamino,§ Toshihisa Tanaka,§ Takashi Kudo,§ Hisashi Tanii,§ Akiko Ikuta,§ Christian Haass,|| and Masatoshi Takeda§

Division of Psychiatry and Behavioral Proteomics, Department of Post-Genomics and Diseases, Osaka University Graduate School of Medicine, Osaka, Japan, and Adolf Butenandt Institute, Department of Biochemistry, Laboratory for Alzheimer's and Parkinson's Disease Research, Ludwig-Maximilians University, Munich, Germany

Received November 25, 2005; Revised Manuscript Received February 25, 2006

ABSTRACT: The presenilin (PS)/γ-secretase complex, which contains not only PS but also Aph-1, PEN-2, and nicastrin, mediates proteolysis of the transmembrane domain of β-amyloid protein precursor (βAPP). Intramembrane proteolysis occurs at the interface between the membrane and cytosol (ε-site) and near the middle of the transmembrane domain (γ-site), generating the βAPP intracellular domain (AICD) and Alzheimer disease-associated Aβ, respectively. Both cleavage sites exhibit some diversity. Changes in the precision of γ-cleavage, which potentially results in secretion of pathogenic Aβ42, have been intensively studied, while those of ε-cleavage have not. Although a number of PS-associated factors have been identified, it is unclear whether any of them physiologically regulate the precision of cleavage by PS/γ-secretase. Moreover, there is currently no clear evidence of whether PS/γ-secretase function differs according to the subcellular site. Here, we show that endocytosis affects the precision of PS-dependent ε-cleavage in cell culture. Relative production of longer AICDε49 increases on the plasma membrane, whereas that of shorter AICDε51 increases on endosomes; however, this occurs without a concomitant major change in the precision of cleavage at γ-sites. Moreover, very similar changes in the precision of ε-cleavage are induced by alteration of the pH. Our findings demonstrate that the precision of ε-cleavage by PS/γ-secretase changes depending upon the conditions and the subcellular location. These results suggest that the precision of cleavage by the PS/γ-secretase complex may be physiologically regulated by the subcellular location and conditions.

Intramembrane proteolysis by presenilin (PS)/γ-secretase plays a key role in both Alzheimer disease (AD)[1] and regulated intramembrane proteolysis (RIP) signaling (*1*). At least two PS-dependent cleavages occur in the transmembrane domains of substrates such as β-amyloid protein precursor (βAPP), Notch, and CD44 ("dual cleavage"): one near the middle of the transmembrane domain (TM-N) (*2*−*5*) and the other on the border between the transmembrane domain and cytosol (TM-C) (*6*−*10*). The cleavage at the TM-N site of βAPP (γ-cleavage) is essential for Aβ generation and is closely related to AD (*2*, *11*). On the other hand, the cleavage at the TM-C site, including that in Notch-1 (S3-cleavage), generates ICDs (*i*ntracellular *c*ytoplasmic *d*omains) and is involved in RIP signaling (*1*).

In PS-dependent proteolysis, there is some diversity in the specific sites of cleavage (*3*, *5*, *7*−*9*, *11*). A change in cleavage precision can have an important effect on the pathogenesis of AD because Aβ42, a causative factor in AD, is generated by one of the types of γ-cleavage (*2*, *11*). Much time and effort have therefore been dedicated to understanding how the precise site of cleavage is determined. Most familial AD-associated PS and βAPP mutants affect the precision of γ-cleavage (*11*). Because such changes in the precision of γ-cleavage have not been observed in other conditions, it had been generally believed that the precision of this cleavage is not easily changed (*11*). Recent studies, however, have revealed that some chemicals including NSAIDs (*n*onsteroidal *a*nti*i*nflammatory *d*rugs) (*12*, *13*) up- or downregulate pathological Aβ42, indicating that the precision of this cleavage by PS/γ-secretase may change under certain circumstances (*14*). Notably, however, corresponding changes in the precision of ε-cleavage have not been examined.

ICDs including that of βAPP (AICD) and Notch (NICD) are generated by ε- and S3-cleavage at TM-C, respectively (*1*). ICDs are generally involved in translocation of signaling

† This work was supported by the Program for the Promotion of Fundamental Studies in Health Sciences of the National Institute of Biomedical Innovation (05-26), by Grants-in-Aid for Scientific Research on Priority Areas−Advanced Brain Science Project and for KAKENHI from the Ministry of Education, Culture, Sports, Science, and Technology of Japan, and by Grants-in-Aid from the Ministry of Health, Labor, and Welfare of Japan.

* To whom correspondence should be addressed. Tel: 81-6-6879-3053. Fax: 81-6-6879-3059. E-mail: mokochi@psy.med.osaka-u.ac.jp.

‡ Equal contributions.

§ Osaka University Graduate School of Medicine.

|| Ludwig-Maximilians University.

[1] Abbreviations: Aβ, amyloid-β peptide; AD, Alzheimer disease; AICD, βAPP intracellular cytoplasmic domain; βAPP, β-amyloid protein precursor; CMF, crude membrane fraction; CTF, carboxyl-terminal fragment; Dyn-1, dynamin-1; IP-MS, immunoprecipitation−mass spectroscopy; K293, human embryonic kidney 293; PM, plasma membrane; PS, presenilin; sw, Swedish mutant; TM-C, the border between the transmembrane domain and cytosol.

10.1021/bi052412w CCC: $33.50
Published on Web 03/28/2006

molecules to the nucleus to activate target genes in RIP signaling (*1*). Although, like γ-cleavage, ϵ-cleavage also exhibits diversity (*7*−*9*), the details of this diversity and the characteristics of the cleavage remain to be clarified. Both ϵ- and γ-cleavages are mediated by PS/γ-secretase (*2*), but whether the processes that determine the variety and the precision of these cleavages are common remains controversial. For example, it has been shown that ϵ-cleavage sites are associated with γ-cleavage sites (*7*, *15*, *16*); however, mutagenesis studies show that ϵ- and γ-cleavages are mediated by a distinct process (*17*).

PS is the proteolytic active center in the PS/γ-secretase protein complex (*2*, *18*). To exert its proteolytic function, PS must form a complex with at least nicastrin (*19*), PEN-2 (*20*), and APH-1 (*2*, *20*). Other factors that physiologically affect proteolysis, including the precision of cleavage, have not yet been identified. In contrast to other subcellular locations, AD-associated Aβ42 is produced in the ER without concomitant production of Aβ40. However, since this is not mediated by PS (*21*, *22*), whether the precision of PS-dependent proteolysis changes within cells depending on location or conditions remains unresolved.

In this study, using a cell-free γ-secretase assay, we examined whether the precision of cleavage by PS/γ-secretase is affected by its subcellular location. We demonstrate that, unlike γ-cleavage, ϵ-cleavage precision can drastically change depending on subcellular location and the pH. Relative cleavage at the ϵ51 site is more prone to occur on endosomes than on plasma membrane (PM) and at lower pH. In contrast, relative cleavage at the ϵ49 site is more likely to occur on PM than on endosomes and at higher pH. These results suggest that PS-dependent γ-secretase on plasma membrane and endosomes is functionally distinct.

MATERIALS AND METHODS

Antibodies. Rabbit antiserum 6618 was raised against a synthetic peptide KMQQNGYENPTYKFFEQMQN, which corresponds to the C-terminus of βAPP according to the methods described (*23*). The following antibodies were purchased from commercial sources: anti-Aβ antibody 4G8 (Senetec PLC), anti-Na−K ATPase (Upstate Biotechnology), anti-early endosome antigen 1 (BD Transduction Laboratories), anti-nicastrin (Sigma-Aldrich), anti-GM130 (BD Transduction Laboratories), and anti-tubulin (Santa Cruz Biotechnology). Also, antibody 12CA5 (Roche Diagnostics Inc.) was used to detect the N-terminal hemagglutinin-tagged dynamin-1 (Dyn-1) K44A mutant.

Cell Culture and cDNA Construct. Human embryonic kidney 293 (K293) cells stably expressing wild-type βAPP, wild-type PS1/βAPP Swedish (sw) mutant (*24*), or PS1 D385N/βAPP sw (*25*) were described previously. HeLa cells expressing Dyn-1 K44A under control of a tetracycline transactivator were kindly provided by Dr. Sandra L. Schmid (Scripps Institute, La Jolla, CA) (*26*). HeLa cells stably expressing βAPP sw were cultured without tetracycline (Sigma-Aldrich) for 48 h to induce expression of Dyn-1 K44A.

Membrane Fractionation and Cell-Free γ-Secretase Assay. The collected cells were homogenized with a Teflon homogenizer (20 strokes) in homogenization buffer (0.25 M sucrose and 10 mM HEPES, pH 7.4) containing a protease inhibitor cocktail (Roche) (*27*). The homogenate was centrifuged at 1000*g* for 5 min to remove nuclei and cell debris, followed by further centrifugation of the supernatant fraction at 100000*g* for 1 h. Following a single wash with homogenization buffer, the resulting precipitate was collected as the CMF and frozen in liquid nitrogen. Upon use, the frozen CMF samples were resuspended and immediately incubated in the reaction buffer [150 mM sodium citrate buffer (pH 5.0−7.4) containing 5 mM 1,10-phenanthroline (Sigma-Aldrich) and a 4× concentration of protease inhibitor cocktail (Roche)] for 20 min at 37 °C (cell-free incubation) (*28*, *29*). The reaction was terminated by placing the samples on ice.

Subcellular Fractionation. Linear gradients of 2.5−25% iodixanol (Optiprep; AXIS-SHIELD) were prepared. Postnuclear supernatant fractions from 24 dishes (ϕ = 14 cm) were loaded on the top of the gradient, followed by centrifugation for 3 h at 130000*g*. Each fraction was diluted with three volumes of homogenization buffer and centrifuged for 1 h at 100000*g* to precipitate the membranes. The precipitated membrane was used in cell-free γ-secretase assays or in immunoblots for marker proteins.

Metabolic Labeling. Following methionine starvation for 40 min, cells were metabolically labeled with 400 μCi of [^{35}S]methionine (Redivue Promix; Amersham Pharmacia Biotech) in methionine-free MEM for 20 min and chased for 30 min in DMEM containing 10% FBS and excess unlabeled methionine.

Immunoprecipitation/Autoradiography Analysis. Metabolically labeled CMF was lysed in RIPA buffer (1% Triton X-100, 0.5% sodium deoxycholate, and 0.1% SDS) containing a protease inhibitor mix (Sigma-Aldrich). The cell lysates were centrifuged at 10000*g* for 15 min, and the supernatant fractions were immunoprecipitated with 6618 antiserum for the detection of the C-terminal stub and de novo AICD. Following 10−20% Tris−tricine SDS−PAGE (Invitrogen), the gels were dried and analyzed by autoradiography (*3*).

Immunoprecipitation/Mass Spectroscopy (IP-MS) Analysis. IP-MS analysis was carried out as described previously (*3*). Following cell-free incubation, the CMF was sonicated four times for 10 s and then centrifuged at 100000*g* for 1 h. The supernatant were immunoprecipitated for 4 h at 4 °C in IP-MS buffer [140 mM NaCl, 0.1% *n*-octyl glucoside, 10 mM Tris-HCl (pH 8.0), 5 mM EDTA, and a protease inhibitor mix (Sigma-Aldrich)]. The heights of the MS peaks and molecular weights were calibrated using ubiquitin and/or bovine insulin β-chain as standards (Sigma-Aldrich). The relative peak heights were semiquantitatively analyzed (see Figure 3 in Supporting Information).

Immunoprecipitation/Immunoblot Analysis. Following cell-free incubation, the fractions were immunoprecipitated for 10 h at 4 °C in IP-MS buffer. After SDS−PAGE, the separated proteins were transferred to a PVDF or nitrocellulose (for detection of Aβ) membrane and probed with the indicated antibodies (*30*). The nitrocellulose membrane was heated for 10 min in boiling PBS before blocking. AICD and Aβ levels were semiquantified by chemiluminescence using an LAS3000 scanner and Multi Gauge Ver3.0 software (Fujifilm).

Transferrin Uptake Assay. To determine the level of internalized transferrin, the treated cells were washed three times in Hank's balanced salt solution (Sigma-Aldrich), pH 7.4, and then treated for 7 min at 37 °C with 8 μg/mL biotin−

transferrin (Sigma-Aldrich) in conditioned medium. To remove remaining surface-bound biotin−transferrin, cells were washed three times with Hank's balanced salt solution, pH 4.0. To determine the level of surface-bound transferrin, the treated cells were incubated for 30 min with biotin−transferrin at 4 °C and washed three times with Hank's balanced salt solution, pH 7.4 (*26*). The resulting cell lysates were separated by SDS−PAGE and transferred to the PVDF membrane. Biotin−transferrin was detected by neutravidin−horseradish peroxidase (Pierce). The level of endocytosis in each condition was expressed as of the ratio of internalized vs surface-bound transferrin (*31*).

RESULTS

The Cell-Free Assay Constitutes Bona Fide ϵ- and γ-Cleavages by PS/γ-Secretase. βAPP, a type 1 transmembrane protein, undergoes PS-dependent proteolysis in its transmembrane domain, following "shedding" of the extracellular domain at β- or α-sites (*11*). The intramembrane proteolysis is composed of at least two distinct proteolytic cleavages (dual cleavage), namely, at the ϵ- and γ-sites (Figure 1A) (*2*).

To determine whether the precision of cleavage in intramembrane proteolysis by each PS/γ-secretase is homogeneous in cells, we established a cell-free γ-secretase assay using a detergent-free membrane fraction (Figure 1) (*28*). First, de novo AICD generation from carboxyl-terminal fragment (CTF) stubs of βAPP was analyzed (Figure 1B,C). Following a 20 min metabolic labeling of K293 cells stably expressing βAPP sw and a 30 min chase, we extracted CMFs from the cells and incubated them under various conditions (cell-free incubation). To detect the C-terminus of βAPP, cell lysates were immunoprecipitated with rabbit antiserum 6618, separated by SDS−PAGE, and analyzed by autoradiography. As shown in Figure 1B, during cell-free incubation of the purified CMF, radiolabeled CTF stubs of βAPP rapidly underwent endoproteolysis and concomitantly generated labeled AICD. Termination of the PS function by either exogenous expression of the PS1 dominant negative mutant (D385N) (*32*) or by addition of a specific γ-secretase inhibitor to CMF (Figure 1C) inhibited generation of AICD.

We next examined the precision of both ϵ- and γ-cleavages in the cell-free assay using IP-MS analysis (Figure 1D). We first examined the molecular species of AICD generated during cell-free incubation. The IP-MS analysis showed that the MS profile of AICD was consistent with that previously reported (Figure 1D, left panel) (*7*−*9*). In addition, the MS spectrum of Aβ generated during cell-free incubation (Figure 1D, right panel) was almost identical to that of Aβ present in the conditioned medium just before extraction of the CMF (data not shown). We therefore conclude that the cleavages in the cell-free assay constitute bona fide PS-dependent ϵ- and γ-cleavages (Figure 1E).

The Precision of ϵ-Cleavage Drastically Changes upon Inhibition of Endocytosis. Proteolysis by PS/γ-secretase occurs on cell organelles including the PM and endosomes before and after endocytosis (*33*). Here, we focused on whether the precision of ϵ- and γ-cleavage changes upon inhibition of endocytosis. To inhibit endocytosis, we used the "tet-off system" (Clontech) in which the expression of the dynamin-1 (Dyn-1) dominant negative mutant K44A is

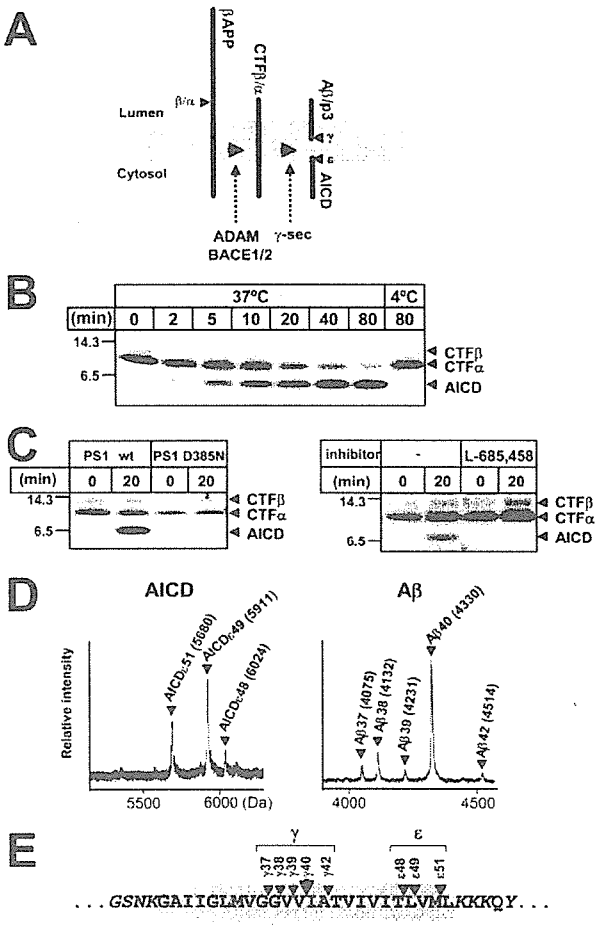

FIGURE 1: Generation of de novo AICD and Aβ in the cell-free γ-secretase assay. (A) Schematic representation of dual cleavage of the βAPP transmembrane domain. See Results for details. (B) Analysis of cell-free γ-secretase assay products by immunoprecipitation/autoradiography using CMF from cells stably expressing βAPP sw. Note that the ~7 kDa product (AICD) was generated over time along with a concurrent reduction in the level of substrates (CTF stubs of βAPP). (C) Analysis of cell-free γ-secretase assay products by immunoprecipitation/autoradiography using CMFs from (i) cells expressing a dominant negative PS1 mutant (PS1 D385N) or (ii) cells treated with or without 10 μM L685,458. (D) Molecular species of de novo AICD and Aβ generated in the cell-free assay. Molecular weights of de novo AICD (left panel) and Aβ (right panel) are shown. Following a 20 min cell-free incubation, the soluble fraction of CMF was immunoprecipitated with antibody 6618 (left panel) or 4G8 (right panel). Panels B−D show representative data from more than three independent experiments. (E) Schematic representation of the ϵ- and γ-cleavages of βAPP. Arrowheads indicate the cleavage sites found in the assay.

induced by tetracycline withdrawal (tet (−) treatment) in HeLa cells (Figure 2A) (*26*). We first examined the extent to which this mutant suppresses endocytosis of the transferrin receptor. We found that expression of Dyn-1 K44A inhibited the intracellular uptake of biotinylated transferrin (Figure 1 in Supporting Information) by approximately 87 ± 2% (Figure 2B).

Next, we analyzed the ϵ-cleavage in the cell-free γ-secretase assay using CMF from cells cultured with or without tetracycline (Figure 2C,D). Unlike the analysis of K293 cells, the mass spectral analysis showed that AICDϵ51 was a major species formed by CMF from HeLa cells stably expressing

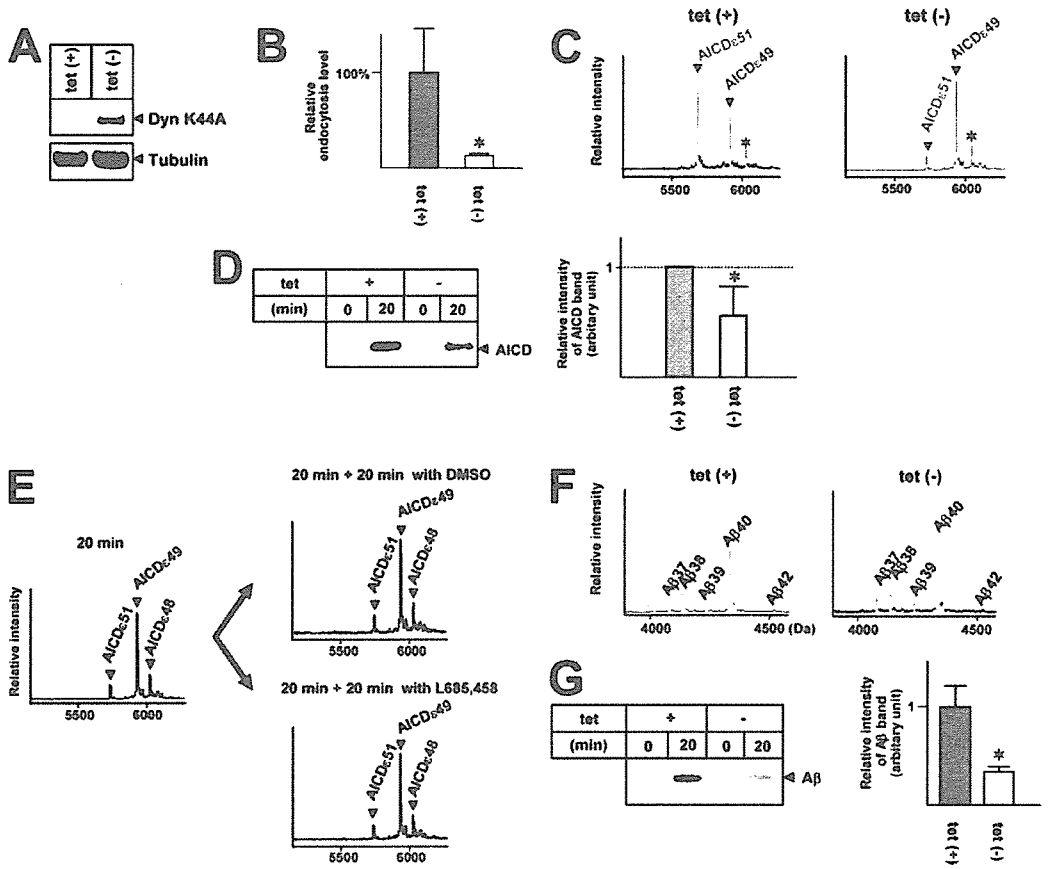

FIGURE 2: Effects of Dyn-1 K44A expression in HeLa cells on the cell-free γ-secretase assay. (A) Induction of Dyn-1 K44A expression. Cells were treated without (−) or with (+) tetracycline, and cell lysates were immunoblotted with 12CA5 (upper panel) or anti-tubulin (lower panel). The results show that Dyn-1 K44A is induced by removal of tetracycline. (B) Inhibition of endocytosis by Dyn-1 K44A expression. The ratio of internalized transferrin at 37 °C to cell surface bound transferrin at 4 °C in cells not expressing Dyn-1 K44A (tet(+)) was defined as 100%. The ratio of endocytosis decreased to 13 ± 2% when the expression of the mutant was induced (tet(−)). The asterisk indicates statistical significance ($P < 0.05$ by Student's t-test). (C) Mass spectra of cell-free generated AICD species. The CMFs from HeLa cells expressing βAPP sw cultured with or without tetracycline were incubated in the cell-free assay. Asterisks indicate the AICDϵ48 species. (D) The level of AICDs generated in the cell-free assay. The AICDs generated in cell-free assays were immunoprecipitated and immunoblotted with the 6618 antiserum (left panel). The intensity of each AICD band was measured by chemiluminescence (right panel). Generation of de novo AICDs was defined as the difference of the AICD band intensities with or without a 20 min cell-free incubation. The asterisk indicates statistical significance ($P < 0.01$ by Student's t-test). (E) Molecular species of AICD observed after a first (left panel) and a second 20 min incubation with L685,458 (lower right panel) or vehicle control DMSO (upper right panel) using CMF from HeLa cells expressing βAPP sw cultured without tetracycline. (F) Mass spectra of the Aβ species generated in the cell-free reaction. The samples were the same as those analyzed in panel C. (G) The level of Aβ produced in the cell-free assay. The Aβ generated in the cell-free assay was analyzed by immunoprecipitation, followed by immunoblotting with the 4G8 antibody (left panel). The intensity of each Aβ band was measured by chemiluminescence (right panel). The asterisk indicates statistical significance ($P < 0.01$ by Student's t-test). In (A), (C), (E), and (F) and in the left panels of (D) and (G), the results are representative data of more than three independent experiments. The results in (B) and the right panels of (D) and (G) indicate the means ± standard deviations of at least triplicate determinations. tet = tetracycline.

βAPP sw in our cell-free assay (Figure 2C, left panel, and Figure 3A, right panel). Surprisingly, expression of Dyn-1 K44A greatly increased the peak height of AICDϵ49 relative to that of AICDϵ51, indicating a change in the precision of ϵ-cleavage upon inhibition of endocytosis (Figure 2C; see also Table 1). A very similar large relative increase of the peak height of AICDϵ49 compared to that of AICDϵ51 was also observed upon addition of 100 nM bafilomycin A1 (Figure 2B in Supporting Information), which inhibited endocytosis by approximately 69 ± 5% (Figures 1 and 2A in Supporting Information) (*34*). Moreover, we found that the relative ratio of the AICDϵ49 peak height to that of AICDϵ51 semiquantitatively correlated with the relative amount of each AICDϵ49 species, indicating that AICDϵ49 and AICDϵ51 have similar ionization efficiencies in the matrix-associated laser desorption ionization/time-of-flight mass spectrometry (see Figure 3 in Supporting Information). We also examined whether the level of ϵ-cleavage changes upon inhibition of endocytosis by immunoblotting (Figure 2D). We detected a significant decrease in intensity of the AICD band upon Dyn-1 K44A expression, indicating that the level of ϵ-cleavage decreases upon inhibition of endocytosis. These findings suggest that inhibition of endocytosis causes a drastic change in the precision of ϵ-cleavage.

We further investigated whether both AICDϵ51 and AICDϵ49 are, indeed, direct products of PS/γ-secretase. We first generated de novo AICD by a 20 min cell-free incubation (Figure 2E, left panel). The solution was further incubated for 20 min with (Figure 2E, lower right panel) or without (Figure 2E, upper right panel) the γ-secretase

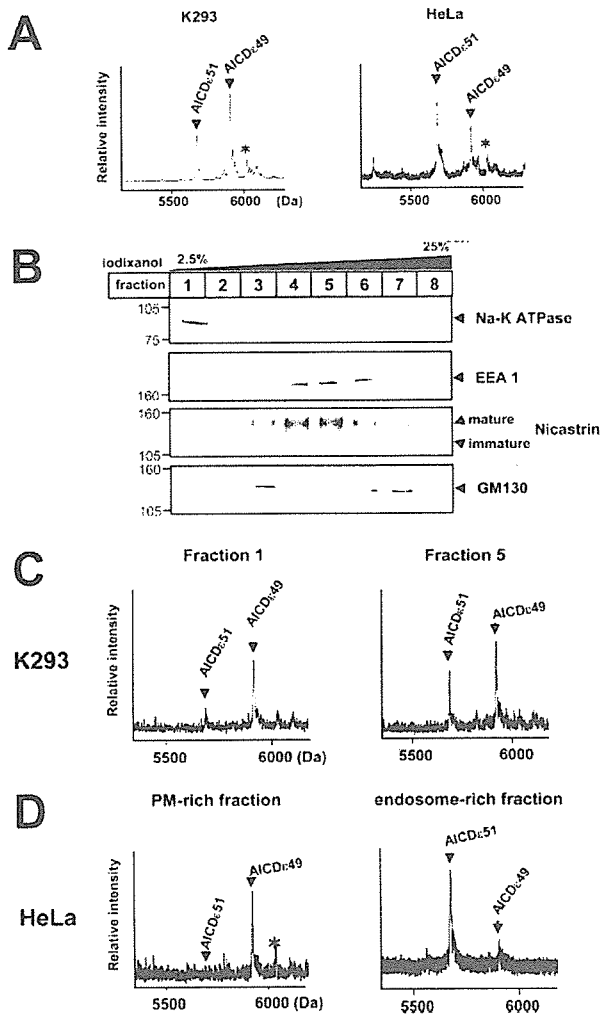

FIGURE 3: Cell-free γ-secretase assay using PM- and endosome-rich fractions. (A) Mass spectra of de novo AICD generated in the cell-free assay using whole CMFs from K293 (left panel) and HeLa (right panel) cells. Asterisks indicate AICDϵ48 species. (B) Postnuclear supernatant fractions of βAPP sw-expressing K293 cells were separated by iodixanol gradient centrifugation and analyzed by immunoblotting using antibodies to organelle marker proteins. (C) Mass spectra of de novo AICD generated by fractions 1 and 5 from K293 cells. (D) Mass spectra of de novo AICD generated by PM- or endosome-rich fractions from HeLa cells expressing βAPP sw. Results in (A) to (D) are representative of more than three independent experiments.

inhibitor L685,458. This inhibitor neither increased the relative peak height of AICDϵ51 nor reduced that of AICDϵ49/AICDϵ48, suggesting that AICDϵ51 is not a degradation product of AICDϵ49/AICDϵ48 but rather is generated directly by PS/γ-secretase.

These results indicated that there is a striking change in the precision of ϵ-cleavage upon inhibition of endocytosis. We therefore examined whether there is also a parallel remarkable change in the precision of γ-cleavage. We chose IP-MS analysis in order to observe all of the de novo Aβ species. In clear contrast to the analysis of AICD (Figure 2C), IP-MS analysis did not reveal drastic differences in the profiles of de novo Aβ species (i.e., Aβ37, Aβ38, Aβ39, Aβ40, and Aβ42) between reactions using CMF from control cells (Figure 2F, left panel) and cells expressing Dyn-1 K44A (Figure 2F, right panel). Also, very similar results were observed upon inhibition of endocytosis by bafilomycin A1 (Figure 2C in Supporting Information). Immunoprecipitation/immunoblotting analysis for detecting Aβ species revealed a significant decrease upon expression of Dyn-1 K44A (Figure 2G). Thus, in parallel to AICD, we detected a decrease in the level of de novo Aβ levels in the presence of Dyn-1 K44A expression. These results indicated a concomitant decrease in both ϵ- and γ-cleavage efficiencies by PS/γ-secretase upon inhibition of endocytosis.

The Precision of ϵ-Cleavage in the PM-Rich Fractions Is Distinct from That in the Endosome-Rich Fractions. Our cell-free γ-secretase assay revealed that inhibition of endocytosis by expression of the Dyn-1 K44A mutant causes a drastic change in the precision of ϵ-cleavage by PS/γ-secretase but does not concurrently cause such a change in the precision of γ-cleavage. This prompted us to investigate whether there are differences in the precision of ϵ-cleavage on the PM and endosomes. Using CMFs from K293 and HeLa cells, we performed cell-free γ-secretase assays and examined the mass spectra of the generated AICD. As described above (Figures 1D and 2C), in unstimulated K293 and HeLa cells, the relative amounts of ϵ49 and ϵ51 produced are different, indicating that the precision of cleavage at the ϵ-site is distinct in the two cell lines (Figure 3A).

We next examined the production of AICD species in PM- and endosome-rich fractions isolated by iodixanol density gradient centrifugation from CMF prepared from K293 cells expressing βAPP sw. Na−K ATPase, a marker of PM, was detected primarily in the lightest fraction (fraction 1; Figure 3B, first panel), whereas the early endosome markers early endosome antigen 1 (Figure 3B, second panel) and matured nicastrin (Figure 3B, third panel) were detected together in higher density fractions (fractions 4 and 5). GM130, a marker of Golgi, was found mainly in fractions 3 and 7 (Figure 3B, fourth panel). These results suggest that fractions 1 and 5 are the PM- and endosome-rich fractions, respectively. When these fractions were employed in the cell-free γ-secretase assay, we found that the peak height of AICDϵ51 relative to that of AICDϵ49 was larger in the endosome-rich fraction than in the PM-rich fraction (Figure 3C). In contrast, the peak height of AICDϵ49 relative to that of AICDϵ51 was higher in the PM-rich fraction than the endosome-rich fraction (Figure 3C). Similarly, using membrane fractions from HeLa cells, we found that AICDϵ49 was the dominant product in PM-rich fractions, whereas AICDϵ51 was the main product in endosome-rich fractions. These results indicate that the precision of ϵ-cleavage differs on PM and endosomes. Specifically, cleavage at ϵ49, which lies deeper inside the transmembrane domain, tends to occur more on PM than endosomes, whereas the opposite is true for cleavage at ϵ51, which lies closer to the cytosolic side and the interface between transmembrane and intracellular domains.

The Precision of ϵ-Cleavage Is Affected by pH. Our results show that the precision of cleavage at the ϵ-site changes drastically upon inhibition of endocytosis and is affected by the subcellular location. The process of cleavage by PS/γ-secretase may therefore change according to the surrounding conditions. For this reason, we examined whether changing the pH during the cell-free γ-secretase assay affects the level and precision of ϵ- and γ-cleavage. IP-MS showed that, when

Table 1: Amino Acid Sequences of AICDϵ49 and AICDϵ51 Species

MW (obsd)	species	sequence	MW (calcd)
5911	AICDϵ49	V^{646}MLKKKQYTSIHHGVVEVDAAVTPEERHLSKMQQNGYENPTYKFFEQMQN^{695}	5910.7
5680	AICDϵ51	L^{648} KKKQYTSIHHGVVEVDAAVTPEERHLSKMQQNGYENPTYKFFEQMQN^{695}	5680.4

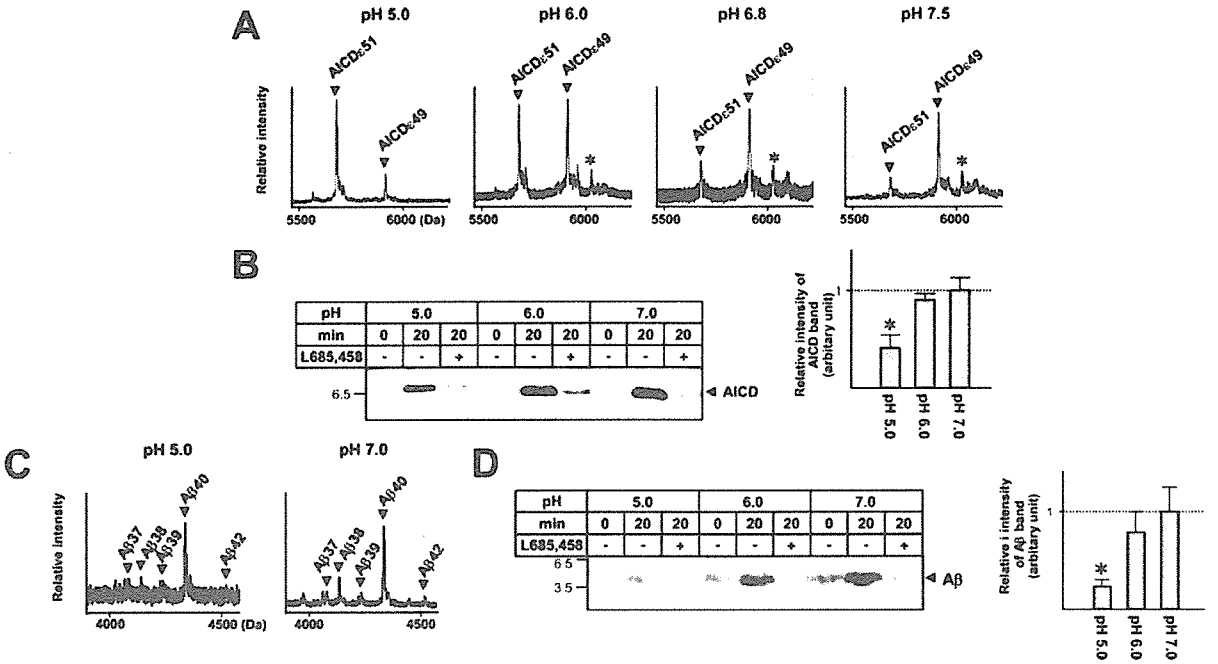

FIGURE 4: Effects of pH on ϵ- and γ-cleavage. (A) Mass spectra of AICD generated in the cell-free assay at pHs between 7.5 and 5.0. CMFs from βAPP sw-expressing K293 cells were resuspended in reaction buffer at the indicated pH. Asterisks indicate AICDϵ48 species. (B) The level of AICDs generated at various pHs. The cell-free incubation was performed in the presence of either L685,458 or vehicle alone (DMSO) (left panel). The asterisk indicates that the intensity of the AICD band at pH 5.0 was statistically lower than those at pH 6.0 and 7.0 ($P < 0.01$ by Student's *t*-test). (C) Mass spectra of Aβ generated in the cell-free assay at pH 5.0 and 7.0. (D) The level of Aβ generated at various pHs and in the presence of L685,458 or vehicle control (DMSO). The asterisk indicates statistical significance ($P < 0.01$ by Student's *t*-test). In (A) and (C) and the left panels of (B) and (D), the results are representative of more than three independent experiments. In the right panels of (B) and (D), the results indicate the means ± standard deviations from at least triplicate determinations.

we changed the buffer pH from 7.5 to 5.0, the relative cleavage efficiency at the ϵ49 and ϵ51 sites changed (Figure 4A). The more acidic the pH, the higher the AICDϵ51 peak became, demonstrating that the pH affects cleavage at the ϵ-site. Immunoblotting also showed that lowering the pH to 5.0 decreased the amount of AICD produced, indicating a reduction in the total amount of cleavage at the ϵ-site (Figure 4B). De novo AICD production was almost completely suppressed by an inhibitor of PS-dependent γ-secretase (L685,458) at various pHs. Therefore, the AICD production that we observed was mostly due to proteolysis by PS-dependent γ-secretase (Figure 4B). These results indicate that alteration of the pH affects both the precision and the level of ϵ-site cleavage. We also studied the effect of pH on the precision and amount of γ-site cleavage. As shown in Figure 4C, we could not detect any ϵ-cleavage-like changes in the precision of γ-cleavage. Also, lowering the pH to 5.0 caused a reduction in the total amount of de novo Aβ production (Figure 4D). Therefore, lowering the pH reduced the level of cleavage at both the γ- and ϵ-sites. Collectively, these results show that the pH in the cell-free assay affects the precision of cleavage at the ϵ-site.

DISCUSSION

In this study, we investigated intramembrane proteolysis of βAPP and demonstrated dynamic changes in the precision of cleavage by the PS/γ-secretase. Using a cell-free γ-secretase assay, we showed that the precision of ϵ-site cleavage changes depending on the subcellular location and pH. These results suggest that the precision of cleavage by the PS/γ-secretase complex can be regulated physiologically.

Inhibition of endocytosis also induced a change in the precision of ϵ-cleavage, suggesting that the function of PS/γ-secretase is related to endocytosis. The precision of ϵ-cleavage on PM and endosomes differs, demonstrating that the function of PS/γ-secretase may be heterogeneous in cells. It is unlikely that the change in precision of ϵ-cleavage observed in this study is due to differences in the thickness of PM and endosome membranes because very similar changes were caused by altering the pH in the cell-free assay. Moreover, our results suggest that the precision of ϵ-cleavage is more dynamic than that of γ-cleavage. Therefore, our results can be explained by (i) additional physiological factors that interact with the active PS/γ-secretase complex or (ii) altered substrate recognition/access at different pH conditions that exist at the plasma membrane and endosomes.

Because the PS/γ-secretase complex mediates both γ- and ϵ-cleavages in the transmembrane domain of βAPP (*2*), one might predict that the processes of γ- and ϵ-cleavage would behave the same. Previous results have shown, however, that the effects of PS mutations on the relative levels of γ42 and